JOURNAL OF GEOPHYSICAL RESEARCH, VOL. 100, NO. C7, PAGES 13,201–13,220, JULY 15, 1995

# A comparison of methods for the measurement of the absorption coefficient in natural waters

W. Scott Pegau,[1] Joan S. Cleveland,[2] W. Doss,[3] C. Dan Kennedy,[4] Robert A. Maffione,[5] James L. Mueller,[2] R. Stone,[3] Charles C. Trees,[2] Alan D. Weidemann,[4] Willard H. Wells,[3] and J. Ronald V. Zaneveld[1]

**Abstract.** In the spring of 1992 an optical closure experiment was conducted at Lake Pend Oreille, Idaho. A primary objective of the experiment was to compare techniques for the measurement of the spectral absorption coefficient and other inherent optical properties of natural waters. Daily averages of absorption coefficients measured using six methods are compared at wavelengths of 456, 488, and 532 nm. Overall agreement was within 40% at 456 nm and improved with increasing wavelength to 25% at 532 nm. These absorption measurements were distributed over the final 9 days of the experiment, when bio-optical conditions in Lake Pend Oreille (as indexed by the beam attenuation coefficient $c_p(660)$ and chlorophyll *a* fluorescence profiles) were representative of those observed throughout the experiment. However, profiles of stimulated chlorophyll *a* fluorescence and beam transmission showed that bio-optical properties in the lake varied strongly on all time and space scales. Therefore environmental variability contributed significantly to deviations between daily mean absorption coefficients measured using the different techniques.

## Introduction

In the spring of 1992 an optical closure experiment was performed at Lake Pend Oreille, Idaho. The experiment was designed to test mathematical relationships between measured sets of several optical properties and to compare results from different techniques used to measure individual optical properties, including the spectral volume absorption coefficient.

Absorption is one of the fundamental processes that determine the shape and magnitude of the light field in a medium. The absorption coefficient is the proportion of the flux lost due to absorption from a beam normal to an infinitesimally thin layer of the medium, divided by the thickness of the layer [e.g., *Jerlov*, 1976]. The absorption coefficient, the volume scattering function, and the input radiance distribution are necessary to solve the radiative transfer equation for the radiance distribution as a function of depth. Thus the absorption coefficient has a key role in determining any optical property that is dependent on the radiance distribution, including the remotely sensed reflectance, the diffuse attenuation coefficient, and irradiance.

In addition to its importance for modeling radiative energy transfer in water, the absorption coefficient is important for studies of phytoplankton productivity and taxonomy. The total absorption coefficient can be partitioned into a sum of the absorption coefficients due to dissolved organic matter, phytoplankton, detrital particles, and water. Spectral characteristics of absorption by phytoplankton result from, and can therefore be used to identify, photosynthetic and auxiliary pigments characteristic of particular phytoplankton taxonomic groups [*Sathyendranath et al.*, 1987]. Investigations and models of primary production must include spectral absorption coefficients of photosynthetic pigments, which determine the ability of phytoplankton to collect light for use in photosynthesis.

The importance of the absorption coefficient and the difficulty of measuring it accurately in low-signal, scattering suspensions has led to the development of a variety of techniques to measure it. In situ measurement techniques include the reflecting tube absorption meter [*Zaneveld et al.*, 1990; *Moore et al.*, 1992], methods that use an isotropic point source [*Sorenson and Honey*, 1968; *Maffione et al.*, 1993], and a number of methods that use a natural light field and *Gershun*'s [1939] equation relating the absorption coefficient to the apparent optical properties [*Tyler*, 1960; *Højerslev*, 1975; *Spitzer and Wernand*, 1981; *Doss and Wells*, 1992; *Voss and Chapin*, 1992; *Voss*, 1989]. Laboratory measurement techniques include the integrating cavity absorption meter [*Fry et al.*, 1992], optoacoustic measurements [*Trees and Voss*, 1990], photothermal measurements [*Bennett et al.*, 1986], and measurements of the component portions using a spectrophotometer [*Yentsch*, 1962; *Kiefer and SooHoo*, 1982; *Roesler et al.*, 1989].

During the April/May 1992 optical closure experiment in Lake Pend Oreille, spectral absorption coefficients were measured using six different techniques, including laboratory measurements that use water samples and in situ measurements. Most of these methods had never been compared. In this paper we compare these techniques for the measurement of the spectral absorption coefficients of natural water and investigate the relative uncertainties between

[1]College of Atmospheric and Oceanic Science, Oregon State University, Corvallis.
[2]Center for Hydro-Optics and Remote Sensing, San Diego State University, San Diego, California.
[3]Tetra Tech Data Systems, Incorporated, Carlsbad, California.
[4]Naval Research Laboratory, Stennis Space Center, Mississippi.
[5]SRI International, Menlo Park, California.



Paper number 95JC00456.
0148-0227/95/95JC-00456$05.00

**Table 1.** The Dates, Wavelengths, and Depths Sampled by Each of the Absorption Techniques

| Instrument | Dates Used | Wavelengths | Depths Sampled |
|---|---|---|---|
| Reflecting tube absorption meter | April 30, May 1, 4, 5, 6, 7 | 456 and 532 nm with 10-nm band-pass filters | approximately every 20 cm from 0 to 80 m, (small-volume measurement) |
| Tethered optical profiler [*Gershun*, 1939] | April 29, 30, May 1, 4, 5, 6, 7 | 440, 453, 486, 518, and 530 nm with 10-nm band-pass filters | 0 to 45 m, maximum depth dependent on wavelength, (large-volume measurement) |
| Isotropic point source | April 23, 24, 27, 28, 29, 30, May 1, 4, 5, 6, 7 | 456, 488, and 532 nm with 10-nm band-pass filters | discrete samples between 10 and 90 m, sample size 10 to 15 m, (large-volume measurement) |
| Compound radiometer | May 1 | 450 nm with 10-nm band-pass filters | 5 to 25 m (large-volume measurement) |
| Integrating cavity absorption meter | April 27, 28, 29, 30, May 1 | 440, 456, 488, 532, 565, 600, 630, 676, and 712 nm with 3-nm band-pass | discrete water samples taken from 5 to 100 m (small-volume measurement) |
| Spectrophotometer | April 23, 24, 27, 28, 29, 30, May 1, 4, 5, 6, 7 | 400 to 700 nm every nanometer with 4-nm band-pass | discrete water samples taken from 5 to 100 m (small-volume measurement) |

methods. We also examine the data for evidence of systematic deviations in absorption estimates which may result from the different measurement volumes, calibration techniques, and wavelength band-pass characteristics of the methods.

The Lake Pend Oreille site was selected primarily because *Tyler*'s [1960] optical measurements there indicated that in late winter and early spring we could expect to find a well-mixed water column having a relatively homogeneous distribution of bio-optical properties. Unfortunately, the spring of 1992 was an unusually warm season and the lake had begun to stratify both thermally and bio-optically. These conditions resulted in significant spatial and temporal variability which detracted from our comparisons, but which made the lake a more typical optical environment.

A second important consideration in our choice of this site was the availability of a Navy barge moored in 200 m of water, which provided an ideal platform from which to deploy several optical systems simultaneously. It is rarely possible to deploy more than one measurement system at a time from a research vessel at sea. The barge and other essential logistical support facilities are maintained by the Acoustic Research Detachment of the U.S. Navy's David Taylor Research Center (DTRC) in and near Bayview, Idaho.

## Methods

The six individual absorption measurement techniques used in the optical closure experiment and ancillary measurements made to characterize bio-optical variability associated with particles are briefly described in this section. The absorption measurement systems, in the order described below, are the reflecting tube absorption meter (RTAM), the tethered optical profiling system (TOPS), the isotropic point source (IPS), the compound radiometer (CR), the integrating cavity absorption meter (ICAM), and a spectrophotometer. The three wavelengths at which most of the instruments were operated were 456, 488, and 532 nm. Dates, measurement wavelengths, and sampling depths for each absorption measurement system are listed in Table 1. The IPS, spectrophotometer, and TOPS were the only techniques with which measurements were made at all three wavelengths for the period of April 30 to May 7. A 456-nm RTAM was operated from April 30 to May 5, and a 532-nm RTAM was operated on all days. At depths below 50 m, where the IPS method worked best, absorption coefficients determined with the IPS, spectrophotometer, ICAM, and the two RTAMs are compared. Absorption measurements by the TOPS, RTAMs, ICAM, CR, and spectrophotometer are compared in the upper 30 m of the water column. Measurements by the IPS and TOPS, which both integrate absorption over large water volumes, cannot be compared directly, because the TOPS measurements require strong ambient daylight and the IPS requires near or total darkness to derive accurate absorption coefficients.

### Sampling Site

We conducted the optical closure experiment from a Navy barge operated by the David Taylor Research Center located in Bayview, Idaho. The barge, moored in Scenic Bay, Lake Pend Oreille, in approximately 200 m of water (Figure 1), is 145 feet (44.2 m) long and 78 feet (23.8 m) wide. A 22 feet (6.7 m) wide by 125 feet (38.1 m) long well runs through the center of the barge and is open at its eastern end (Figure 2).

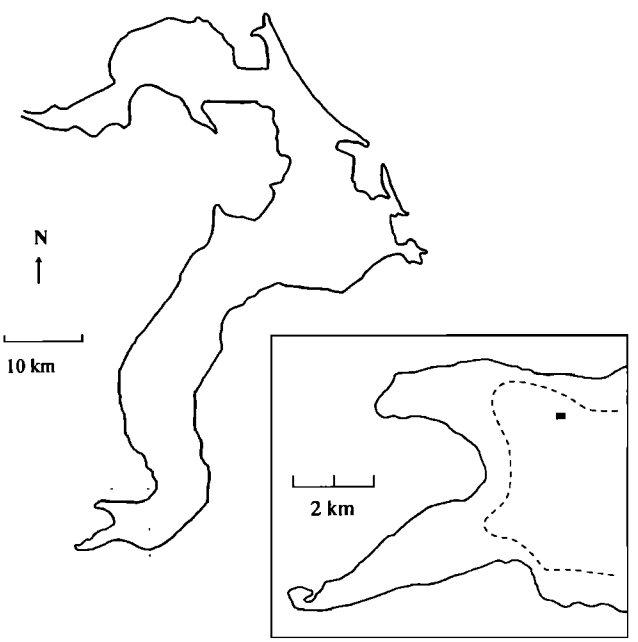


**Figure 1.** Map of Lake Pend Oreille, Idaho. The inset is of Scenic Bay, the dotted line represents the 100-m isobath, and the square is the location of the barge.

The enclosed portion at the western edge of the barge contained wet and dry laboratories. A second, smaller barge, containing electrical power transformers, was moored to the western end of the large barge.

Water samples (taken with 8-L Niskin bottles attached to the conductivity-temperature-depth (CTD) wire) and the reflecting tube absorption meter measurements were taken at the western end of the well (Figure 2). The IPS was deployed from a platform spanning the open well 10 m away from the CTD deployment location. The CR was operated at the eastern end of the barge. A haul-down mooring was used to deploy the TOPS irradiance sensors about 150 m SW of the barge, well away from possible light reflections and shadowing by the barge.

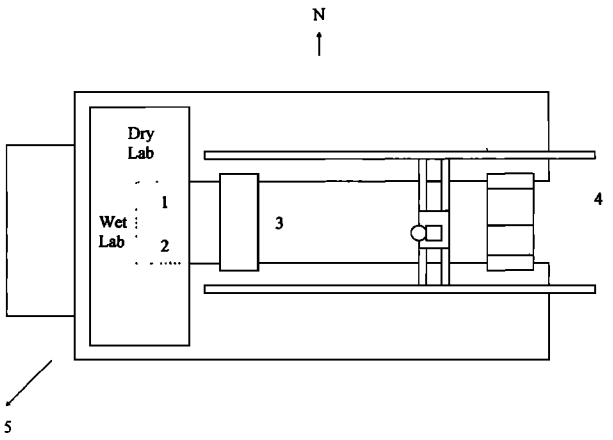


**Figure 2.** Layout of the barge, including locations where the different instruments were used as follows: (1) the reflecting tube absorption meters, (2) the conductivity-temperature-depth (CTD) with water samples for the spectrophotometer and integrating cavity absorption meter, (3) the isotropic point source, (4) the compound radiometer, and (5) the tethered optical profiling system (TOPS) haul-down where vector and scalar irradiance measurements were made.

### Ancillary Measurements

**Beam attenuation at 660 nm and in situ chlorophyll *a* fluorescence.** Beam attenuation at 660 nm (reported as the particulate portion of the beam attenuation coefficient [$c_p(660) = c(660) - c_{water}(660)$]) and chlorophyll *a* fluorescence (reported as fluorometer voltage) were measured using Sea Tech, Inc., instruments located on the TOPS haul-down platform and on the CTD. A third fluorometer was attached to the instrument cage on which the reflecting tube absorption meters were mounted. These instrument packages were lowered and raised several times each day to obtain vertical profiles of optical properties, both within the well and outside of the influence of the barge. The time series of $c_p(660)$ and in situ chlorophyll *a* fluorescence provide estimates of the relative magnitudes of temporal variability in particulate concentrations and bio-optical properties within the water column at fixed horizontal positions in the lake.

**Chlorophyll *a* concentrations.** Chlorophyll *a* concentrations were determined for water samples taken from Niskin bottle casts, typically twice daily at several discrete depths. The water samples were filtered through Whatman GF/F glass-fiber filters, and pigments were extracted in 90% acetone. Chlorophyll *a* concentrations reported here were measured using the standard fluorometric method [*Strickland and Parsons*, 1972], although the pigment concentrations in each sample were also measured using the high-performance liquid chromatography (HPLC) method. Fluorometric chlorophyll *a* concentrations generally overestimated the HPLC concentration. The two measures are related by the regression equation Chl(fluorometric) = 0.025 + 1.115 Chl(HPLC) ($r^2 = 0.934$).

### In Situ Absorption Measurements

**Reflecting tube absorption meter (RTAM).** The RTAM uses a collimated beam light source and encloses the sample in a reflective tube. The reflective tube collects the near-forward scattered light so that the radiant flux lost due to absorption may be estimated [*Zaneveld et al.*, 1990]. These instruments actually measure the absorption coefficient plus a small portion of the scattering coefficient associated with the uncollected scattered light. The uncorrected absorption coefficient $a_u$ is obtained using:

$$a_u = -\frac{1}{L} \ln \left( \frac{V_{samp}}{V_{pw}} \right), \tag{1}$$

where $L$ is the path length of the instrument, $V_{samp}$ is the signal voltage for the sample, and $V_{pw}$ is the signal voltage for pure water. Note that this is essentially the same approach as is used in a spectrophotometer. Rather than using a reference cell, the meter is calibrated in the laboratory. Algorithms using simultaneous measurements of the beam attenuation coefficient are then applied to remove the portion of the scattering coefficient included in the signal [*Zaneveld et al.*, 1992]. We used the "standard" correction scheme described by *Zaneveld et al.* [1992],

$$a_{total} = a_u + 0.13b + a_{water}, \tag{2}$$

where $b$ is the total scattering coefficient. In order to determine the total absorption coefficient, we used the pure water absorption coefficients of *Smith and Baker* [1981].

Three RTAMs were used to determine absorption coefficients at wavelengths of 456, 488, and 532 nm during the closure experiment. Each of these instruments, manufactured by Sea Tech, Inc., measures absorption over a 25-cm path length at a single wavelength. The RTAMs were sampled at a frequency of 1 Hz and were lowered and raised at a rate to measure vertical absorption profiles with approximately 0.2-m resolution.

**Gershun's equation.** Several of the in situ methods for determining the spectral absorption coefficient are based on the following relationship, due to *Gershun* [1939];

$$-\nabla \cdot E(r) = a(r)E_o(r), \tag{3}$$

where $E$ is the vector irradiance and $E_o$ is the scalar irradiance. The steady state plane parallel approximation to (3) can be written as:

$$a(\lambda, z) = K(\lambda, z)\bar{\mu}(\lambda, z), \tag{4}$$

where $K = -1/E\ (dE/dz)$ and $\bar{\mu} = E/E_o$. Vertical profiles of the vector and scalar irradiance are used to determine $K$ and $\bar{\mu}$. Several methods have been used to measure $E$ and $E_o$. Vertical profiles of the radiance distribution can be integrated to obtain vertical profiles of $E$ and $E_o$ and hence

$K$ and $\bar{\mu}$ (e.g., *Tyler* [1960], also in Lake Pend Oreille). Vector and scalar irradiance fields can be determined more directly from direct measures of their upwelling and downwelling components using calibrated detectors equipped with cosine response and spherical irradiance collectors. A third approach, proposed by *Gershun* [1939] and first implemented by *Højerslev* [1975], uses two detectors equipped with spherical irradiance collectors oriented in opposing directions, masked so that they each collect light over one hemisphere. When the detectors are aligned in the vertical direction, the upper collector measures a combined hemispherical irradiance given by

$$E_{hl} \propto 0.5(E_o + E) \tag{5}$$

and the lower hemispherical collector measures a hemispherical irradiance of

$$E_{hl} \propto 0.5(E_o - E). \tag{6}$$

Assuming only a relative calibration of the two detectors, values proportional to the vector and scalar irradiances can then be determined by solving (5) and (6). When the absorption coefficient is determined from these quantities using (3), the proportionality constants cancel (along with any absolute calibration error). The next three sections describe water measurement techniques that use some form of Gershun's equation.

**Tethered optical profiling system (TOPS).** Vertical profiles of spectral vector and scalar irradiance and radiance, as well as $c(660, z)$ and chlorophyll *a* fluorescence $F(z)$, were measured from a buoyant multiple radiometer package, called the tethered optical profiling system (TOPS). The TOPS instrument suite was mounted on an inverted triangular frame (flat edge parallel to the water surface) with each side approximately 3 m long. A line attached to the frame was passed through a block mounted on a mooring anchor at approximately 200 m depth and up to a winch on the barge. This arrangement allowed downward profiles to be obtained by pulling the platform down in the water column. Upward profiles were obtained by floating the positively buoyant system to the surface of the lake. The frame was ballasted to provide proper orientation of the radiometers throughout the profile.

A MER1032 radiometer was attached to one end of the top bar to measure $E_d(\lambda, z)$, $E_u(\lambda, z)$, and $L_u(\lambda, z)$. At the other end of the bar, a MER2040 equipped with spherical collectors was mounted to measure the scalar irradiances $E_{od}(\lambda, z)$ and $E_{ou}(\lambda, z)$. The MER1032 and MER2040 are commercially available, underwater profiling, multichannel filter radiometers manufactured by Biospherical Instruments, Inc. Surface irradiance measurements were made high in the barge superstructure using a five-channel radiometer.

The TOPS $E_d(\lambda, z)$, $E_u(\lambda, z)$, $L_u(\lambda, z)$, and $E_o(\lambda, z)$ profiles were analyzed to determine $K(\lambda, z)$ and the value of each parameter just below the water surface using the integral least squares finite element method of *Mueller* [1991]. The data were then applied to (4) in order to obtain estimates of the absorption coefficient.

The estimation of scalar irradiance from the MER2040 with glass spherical diffusers was not straightforward. The optical configurations of the uplooking and downlooking collector assemblies differed from each other, and the collector surfaces were converted to hemispheres (using opaque plastic tape to mask the lower half of the globe) on May 5. Only the uplooking collector measurements were used for the present analysis.

The uplooking collector was configured by placing the glass diffuser globe directly over the MER2040's cosine collector. In this configuration the unit has relatively uniform directional response to incident irradiance, except for the cone blocked by the instrument body itself (approximately a 1.83-sr solid angle centered on nadir). Assuming the radiance is constant over the blocked cone, we may use the upwelling radiance measured by the MER1032 to correct for the blocked portion of the light field

$$E_o(\lambda, z) = E_{od}(\lambda, z) + 1.8302L_u(\lambda, z). \tag{7}$$

When the uplooking collector was configured as a hemisphere, its response was that given by (5). Using $E(\lambda, z)$ measured with the MER1032, scalar irradiance may be computed as

$$E_o(\lambda, z) = 2E_{hl}(\lambda, z) - E(\lambda, z), \tag{8}$$

where $E_{hl}(\lambda, z)$ is the measured irradiance using the hemispherical configuration of the uplooking collector.

The MER1032, MER2040, and five-channel surface irradiance radiometers were calibrated and characterized using the methods described by *Mueller and Austin* [1992]. The internal uncertainty in the radiometric irradiance/radiance responsivities of the MER1032 and five-channel surface radiometers, based on pre-, intermediate, and postexperiment calibrations and internal consistency checks during individual calibrations, is <2% in all channels. Owing to electronic noise in the MER2040, the internal calibration uncertainty for the channels of this instrument ranged from 5% to 7%. This electronic noise was subsequently traced to a floating ground in the electronic boards of this particular MER2040.

To characterize the directional response of the hemispherical $E_{hd}$ collectors, the MER2040 was illuminated by a National Institute of Standards and Technology traceable spectral irradiance standard at a distance of 150 cm. The instrument was rotated in 10° zenith increments from vertical to horizontal illumination. At each zenith angle, six readings were obtained by rotating the instrument through 60° increments in azimuth. Standard deviations in these samples were typically 7% of the mean response, which is attributed to the electrical noise discussed in the previous paragraph. The variations in the instrument's relative response followed [1 + cos ($\theta$)]/2 to within ±5% (average of the 490 and 532 channels; there was insufficient flux at 456 nm for this laboratory test). The directional response of this collector was not determined for the $E_{od}$ configuration, and we have assumed that uncertainty is similar to that for $E_{hd}$.

The MER2040 was postcalibrated with the spherical collectors filled with water filtered by a reverse osmosis system. In the field at Lake Pend Oreille we attempted to fill the globes with reverse osmosis filtered water, but unfortunately, small amounts of lake water leaked into the globes during each of three TOPS system reconfigurations and redeployments on April 29, May 1, and May 5, 1992. Absorption by chlorophyll, other particulates, and dissolved organic material therefore reduced the radiometric responsivities of the MER2040 spherical and hemispherical irradi-

ance channels by some amount during each deployment period. To estimate a minimum adjustment to the $E_{od}$ (and $E_{hd}$) channels, we assumed that the mean cosine just beneath the sea surface should be constrained to be less than or equal to the cosine of the refracted solar zenith angle. For each deployment period we extracted smoothed surface values and computed the $E_{od}$ (or $E_{hd}$) adjustment factors at (456, 488, and 532 nm) required to satisfy this mean cosine constraint and averaged to obtain [1.29 (0.09), 1.21 (0.07), and 1.12 (0.07)] for April 29 and 30 $E_{od}$ measurements [1.17 (0.08), 1.11 (0.07), and 1.05 (0.08)] for May 1–5, 1992, $E_{od}$ measurements, and [1.22 (0.08), 1.19 (0.09), and 1.14 (0.08)] for May 5–7 $E_{hd}$ measurements. $E_{od}$ or $E_{hd}$ were multiplied by these factors prior to using (7) or (8), respectively, to compute scalar irradiance $E_o$ at each wavelength. The standard deviations of each scale factor (given in parentheses) are consistent with the approximately 7% internal uncertainty in the radiometric calibration of the MER2040 channels.

**Isotropic point source (IPS).** The isotropic point source (IPS) technique for measuring the in situ absorption coefficient was first proposed by *Sorenson and Honey* [1968]. Basically, they argued that the attenuation of irradiance $E$ from an isotropic source should decay with distance approximately as

$$E(r) \propto \frac{e^{-ar}}{r^2}, \tag{9}$$

where $a$ is the absorption coefficient and $r$ is the radial distance from the source. Thus, by measuring the irradiance from the source as a function of $r$, the absorption coefficient could be determined. The error in this result is the approximation that the path length in the exponent is the geometrical radial distance $r$, when, in fact, scattering increases the mean path by $\delta r$ so that the expression should properly be

$$E(r) \propto \frac{e^{-a(r+\delta r)}}{r^2}. \tag{10}$$

If $\delta r \ll r$, the error will be small.

The vector irradiance (more precisely, the radial component of the vector irradiance) from an isotropic source was rigorously derived from the steady state radiative transfer equation without internal sources by *Maffione et al.* [1993]. Their result is

$$E(r) = \frac{\Phi_0}{4\pi r^2} \exp\left(-a\int_0^r \frac{dr'}{\bar{\mu}}\right), \tag{11}$$

where $\Phi_0$ is the radiant flux emitted by the source and $\bar{\mu}$ is the average cosine of the light field from the source. The only assumption implicit in (11) is that the water column within which $E(r)$ is measured is homogeneous. Equation (11) can be solved for the absorption coefficient giving

$$a = \bar{\mu}\left(-\frac{1}{E}\frac{dE}{dr} - \frac{2}{r}\right) \tag{12a}$$

$$a = \bar{\mu}\left(K_E - \frac{2}{r}\right), \tag{12b}$$

where $K_E$ is the diffuse attenuation coefficient for irradiance.

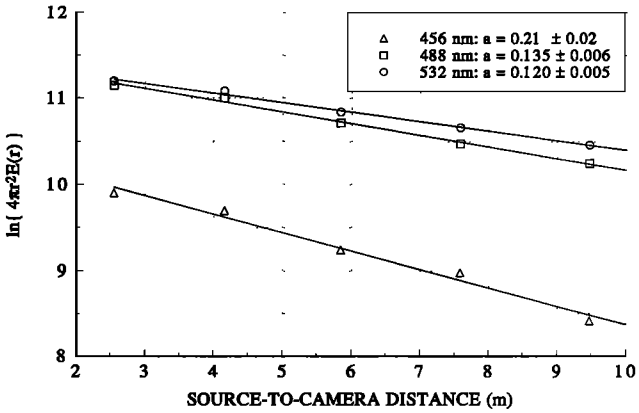


**Figure 3.** Regression fit to attenuation of irradiance from the isotropic source. Slope of the line fit gives the absorption coefficient. Data are from May 6; depth range is 40–50 m.

The similarity of (12b) with the plane-parallel approximation of Gershun's equation, $a = \bar{\mu}K_E$, is no coincidence. In fact, Gershun's equation is a special case of the more general result, equation (12b). In other words, Gershun's equation can be obtained from (12b) in the far field, where $r \to \infty$ and the light field from an isotropic source (e.g., the Sun) becomes plane parallel. Thus methods which use Gershun's equation to determine the absorption coefficient and the IPS method are similar. Both measure a large volume, "integrated" value of $a$, but the IPS method allows the source to be controlled and measurements can be made in both the near and far field. Furthermore, to a good approximation, measurements of $\bar{\mu}$ in the near field are not needed because $\bar{\mu}$ will be approximately equal to 1 (J. S. Jaffe et al., manuscript in preparation, 1994). Thus $a$ can be estimated from measurements of the vector irradiance $E$ alone [*Maffione et al.*, 1991, 1993].

Details of the current implementation of the IPS method are given by *Maffione et al.* [1991, 1993]. To avoid errors due to ambient background light, IPS measurements were made either at night or deep in the water column. To determine the absorption coefficient, irradiance is measured at several distances from an isotropic source. A regression fit to the equation

$$\ln [r^2E(r)] = k - ar, \tag{13}$$

which is derived from the approximate result given by (9) yields the absorption coefficient $a$ as the slope of the regression. An example of the regressions from the data taken at Lake Pend Oreille is shown in Figure 3. Because the IPS method is a variable path length technique (as are all of the large volume methods), the relative error in the estimate of the absorption coefficient can be accurately calculated. This error is shown in the legend of Figure 3 and represents the standard error of the estimate of the slope.

**Compound radiometer (CR).** The CR estimates the absorption coefficient by measuring the moments of a Legendre polynomial expansion of a radiance distribution. The absorption coefficient is determined by applying the measured moments to a form of Gershun's equation [*Zaneveld and Pak*, 1972; *Wells*, 1983]. This device uses a series of reflectors to measure the integral moments of the radiance distribution at a number of zenith angles [*Doss and Wells*,

1992]. The radiance distribution is then deduced from a linear combination of the measured moments. The moments are symmetrical about the vertical axis and optimized to facilitate computation of inherent optical properties in the form of the $A_n$ series as functions of depth, i.e., $A_n(z)$ [*Doss and Wells*, 1992]. The zeroth-order moment ($A_0$) is the absorption coefficient, $A_\infty$ is the beam attenuation coefficient, and the intermediate $A_n$ describe moments of the volume scattering function.

The CR used during this experiment was built and operated by Tetra Tech., Inc. The instrument used at Lake Pend Oreille made measurements on the natural light field, but this instrument can also be used with an artificial light source [*Doss and Wells*, 1992].

### Laboratory Methods

**Integrating cavity absorption meter (ICAM).** The integrating cavity spectral absorption meter is a bench-top instrument for the determination of $a(\lambda)$. Samples of 670 mL each are introduced into a quartz cell within the integrating cavity for measurement. The samples were obtained using the Niskin bottles closed at several depths during each CTD cast in the well.

The theoretical basis of the instrument was developed from an idea put forth by *Elterman* [1970], who built an instrument to measure the absorption of samples of quartz. The theory and a description of the instrumentation is given by *Fry et al.* [1992]. The integrating cavity used at Lake Pend Oreille was of the Texas A&M University design [*Fry et al.*, 1992].

*Fry et al.* [1992] developed a different analysis and calibration scheme than was used for this data set. The calibration scheme and analysis method used for this data set was developed at Naval Research Laboratory (NRL) [*Kennedy*, 1992]. The algorithm developed by NRL calculates an "effective path length" for the cavity. The effective path length is critically dependent on the geometry of the cavity, the refractive index of the sample, and the field of view of the detector [*Kennedy*, 1992]. The measurement is better thought of as a measurement of the change in energy density within the cavity due to the presence of a sample of known volume. Four central assumptions of this measurement are the following. (1) The light field within the cavity is isotropic. Although this cannot be true, it is sufficient that any anisotropy be small, localized, and the same when the cavity is empty. (2) The light field within the sample is isotropic. This assumption breaks down for large absorption values and establishes an upper limit on the cavity's performance. This assumption is valid for all samples taken at Lake Pend Oreille. (3) The change in energy density is due solely to the absorptance of the sample. (4) The absorptance of the empty cavity is zero. However, humid air present during the measurement of the "empty" cavity may cause an offset.

When an empty cavity reading is used as the zero absorptance value, the absorption coefficient can be determined from:

$$a = \frac{1}{\text{effective path length (m)}} \ln\left(\frac{\text{empty}}{\text{sample}}\right). \quad (14)$$

When used in this way, the integrating cavity absorption meter does not require standardization either by measuring known calibration samples with a spectrophotometer or by measuring absorption of "clean" water to determine the total absorption coefficient of the sample. Owing to the long integration times required, the ICAM was not operated in the full spectral mode but at the nine wavelengths given in Table 1.

**Spectrophotometer.** Water samples from the Niskin bottles were analyzed using a spectrophotometer. The spectrophotometer was used to separately measure the particulate and the gelbstoff absorption coefficients. The total absorption coefficient was determined by summing the component contributions with the absorption coefficient of pure water.

The low concentration and absorption signal of suspended particles in the water column requires that the particles be concentrated before their absorption spectrum can be measured in a spectrophotometer [*Yentsch*, 1962]. Water samples (500 to 1130 mL) were filtered through Whatman GF/F (effective pore size, 0.7 $\mu$m) glass-fiber filters. Optical density (OD) spectra (400 to 750 nm) of concentrated particles on the glass-fiber filter [$OD_{filt}(\lambda)$] were measured in a Kontron Uvikon 860 dual-beam scanning spectrophotometer at 4-nm spectral bandwidth using a wet GF/F filter as a blank. Optical density at 750 nm was subtracted from optical density at all other wavelengths. Corrections for path length amplification on the glass-fiber filter and calculations of optical densities for suspensions [$OD_{susp}(\lambda)$] were carried out as described by *Cleveland and Weidemann* [1993] using the empirical equation

$$OD_{susp}(\lambda) = 0.378\ OD_{filt}(\lambda) + 0.523\ OD_{filt}(\lambda)^2. \quad (15)$$

Absorption (in $m^{-1}$) was calculated from optical density as:

$$a_{part}(\lambda) = \frac{A}{V} 2.303\ OD_{susp}(\lambda), \quad (16)$$

where $V$ is the volume filtered (in cubic meters) and $A$ is the clearance area of the filter (in square meters).

Dissolved substances (gelbstoff) are typically defined as those materials passing through a 0.45-$\mu$m filter. However, since particles are defined as the materials collected by a 0.7-$\mu$m filter (described above), this definition of dissolved substances ignores material between 0.45 and 0.7 $\mu$m in size. In order to include all size classes, gelbstoff is defined here as the material passing through a GF/F filter. *Bricaud et al.* [1981] showed that nonlinearity in logarithmic absorption spectra indicates scattering by particles in the dissolved sample; no nonlinearity is seen in these logarithmic absorption spectra. *Bricaud et al.* [1981] used GF/C glass fiber filters, which have an effective pore size of 1.5 $\mu$m. This larger pore size may account for the differences in scattering contamination of dissolved samples.

Filtrate from the concentration of particles on GF/F filters was collected for analysis of absorption by dissolved substances. Optical density spectra (300 to 800 nm) for gelbstoff were measured in 10-cm quartz cuvettes in the Kontron spectrophotometer at 4-nm spectral resolution using a blank consisting of water purified by reverse osmosis. Absorption ($a_{gelb}(\lambda)$) was calculated as:

$$a_{gelb}(\lambda) = 2.303\ OD(\lambda)/l, \quad (17)$$

where $l$ is the path length (in meters).

No baseline adjustments or zero corrections were made to the spectra. The exponential slope for each spectrum was

calculated from absorption between 300 and 450 nm. The mean of these slopes was −0.017 ($n$ = 26, standard deviation = 0.0013, coefficient of variation, 7.6%). Exponential slopes of this magnitude are common in fresh water and coastal waters. Spectral absorption values for all samples were calculated from this slope and the measured absorption at 300 nm:

$$a_{gelb}(\lambda) = a_{gelb}(300) \exp [-0.017(\lambda - 300)]. \quad (18)$$

The total absorption coefficient was calculated at the three wavelengths of interest as:

$$a_t(\lambda) = a_{part}(\lambda) + a_{gelb}(\lambda) + a_w(\lambda), \quad (19)$$

where values of $a_w(\lambda)$ were obtained by interpolation of the results of *Smith and Baker* [1981] to the wavelengths of interest here.

### Instrumental Errors

**RTAM error analysis.** The inherent error in the RTAM approach is due to the undetected scattered light. Various approaches can be used to estimate this undetected light [*Zaneveld et al.*, 1994]. If simultaneous measurements of the spectral absorption and beam attenuation coefficient are made, it can be shown that the error is less than 1% of $b$ [*Zaneveld et al.*, 1994]. The spectral information needed to use these algorithms was not available at Lake Pend Oreille so that the simpler and less accurate correction scheme of (2) was used. Use of this procedure provides a possible error of ±5% of the scattering coefficient. The precision of the instruments was approximately 0.003 $m^{-1}$ so that the details in the vertical structure are well described using this method.

Two problems were encountered in the calibration of this particular set of reflecting tube absorption meters at Lake Pend Oreille. The first is that they displayed some instrumental drift that could not be entirely removed using pure water calibrations. The second problem was cavitation in the flow tubes of the instruments. While both problems degraded the accuracy of the measurements made at Lake Pend Oreille, they were problems with the particular set of instruments and not the method as such. By looking at the deep water ($z$ = 80 m) and correcting for long-term trends using the fluorometer data, it was concluded that the drift yielded an error with a standard deviation of 0.018 $m^{-1}$. Another source of bias, common to all systems that use a pure water reference, is the possibility of contaminated "pure" water used in the calibration and is impossible to estimate.

**TOPS error analysis.** *Gershun*'s [1939, equation (4)] is used with TOPS irradiance profiles to calculate absorption coefficients with an estimated uncertainty of approximately 10%. The dominant uncertainty in TOPS irradiance measurements is an approximately 8% uncertainty in downwelling irradiances measured with the MER2040, either $E_{od}$ with the spherical collector or $E_{ht}$ with the hemispherical collector. This uncertainty includes up to 7% instrument noise observed during the instrument's characterization and calibration, which contributes significantly to the approximately 8% scatter in the "maximum surface mean cosine" adjustments we determined to account for the unknown amounts of lake water which leaked into the collector globe on each of three occasions when the instrument was reconfigured on the mooring. For determining the lake water corrections, TOPS surface irradiances were limited to cases when the solar zenith angle in air ranged between 30 and 50°. Therefore neglect of skylight in our estimates of the maximum surface mean cosine contributed <2% scatter and no significant bias [*Morel*, 1991, Figure 3] to the mean correction coefficients calculated for the MER2040 channels.

Uncertainty in the MER1032 $E_d$ and $E_u$ calibrations, and therefore in $E$, is <2%. Because a single working standard source of spectral irradiance was used to calibrate all irradiance channels on both radiometers, any systematic errors in absolute spectral irradiance responsivity cancel when absorption is computed with *Gershun*'s [1939, equation (4)] ($K$ is independent of an instrument's absolute radiometric responsivity).

The 5% uncertainty in directional response of the $E_{hd}$ collector on the MER2040 (and by assumption of the $E_o$ collector also) is less than the 7% electrical noise of the instrument (as observed during responsivity calibration). We conclude that for this particular instrument, errors in $E_{hd}$ due to this effect are indistinguishable from responsivity noise using normal laboratory sources.

With the $E_{od}$ configuration the excluded integrated solid angle would include 20% to 50% of upward scalar irradiance $E_{ou}$, which is <3% of scalar irradiance [*Voss*, 1989]. We have partially corrected for this discrepancy using radiance measured over a 25° zenith cone with the MER1032 and assuming uniform radiance over a 40° cone. Even assuming this estimate is in error by as much as 30%, this uncertainty contributes <1% uncertainty to scalar irradiance estimated from the MER2040 $E_{od}$ measurements.

Deck cell records show no significant variability due to cloud shadows, and surface wave induced variations were confined to the top 2 m of the water column. Therefore the integral smoothing and $K$ profile analysis [*Mueller*, 1991] should contribute <1% uncertainty in irradiance profiles or $K$ for features in vertical profiles with scales of 4 to 5 m or greater.

**IPS error analysis.** Errors in the IPS method arise from several sources, and all of these errors, except for the assumption of water homogeneity, are due to the particular instrumental implementation and optical conditions in the lake during the experiment. The largest sources of error were (1) the assumption of constant radiant output of the isotropic source during each light flash since a reference detector was not used; (2) variable alignment of the source and detectors due to the variability in water movement; and (3) the assumption that $\bar{\mu} = 1$ since only vector irradiance and not also scalar irradiance was measured. Errors from (1) and (2) should be random and therefore quantified in the standard error of the regression fit. Errors from (2) can also be systematic if instrument misalignment remains constant during a measurement. The error from the assumption that $\bar{\mu} = 1$ is, however, systematic and more difficult to quantify. One thing that can be determined for certain about this systematic error is that it will always lead to an overestimate of $a$. To see this, consider (12) in the form

$$\hat{a} \equiv \frac{a}{\bar{\mu}} = \left(K_E - \frac{2}{r}\right) \quad (20)$$

where $\hat{a}$ is the estimated value of $a$ from the regression fit. The right-hand side of this equation is determined from the vector irradiance measurements alone and used to determine $\hat{a}$, the estimate of $a$. Since $\bar{\mu} \leq 1$, it is clear that $\hat{a} \geq a$. A

Monte Carlo study by Jaffe et al. (manuscript in preparation, 1994) shows that under a wide range of oceanic conditions, $\bar{\mu}$ is nearly always greater than 0.9 up to 10 attenuation lengths from the source. Thus the largest systematic error to be expected in this approximation is about 10%.

Owing to the stratified water above 30 m, absorption values from the IPS method in this region were highly variable and often lower than the other methods. Below this depth the IPS system operated well, except for occasional misalignments between the source and detectors caused by the variable water currents. The error bars on the IPS values in Figures 7–9 represent ±1 standard deviation in the estimate of the slope from the regression fit described in the Methods section. This is a relative error which accounts for random measurement errors but does not take into account systematic error such as a constant misalignment during a measurement run. Nonetheless, some interesting comparisons can be made with the other methods, and the error bars provide an objective indication of the lowest standard deviation in the measurements.

**CR error analysis.** The CR errors depend in a complicated way on the intercalibration of the instrument's 10 optical and detector elements and on the positions of nulls in the spherical harmonics on which the underlying theory is based [*Miles and Wells*, 1993]. In view of this, the best estimates of errors are indirect. The CR measures not only absorption, but also eight integral moments of the scattering function, $A_0$ through $A_8$, as defined by *Wells* [1983] and repeated by *Doss and Wells* [1992]. The $A_n$ series is known from fundamental principles to be a smooth function of $n$, and so the deviation of calculated $a = A_0$ from a smooth fit provides the best estimate of error, as shown by *Miles and Wells* [1993, Figure 1]. Their results predict an uncertainty of $\approx 0.01\ m^{-1}$ in the depth range of 12 to 18 m. This is the range in which the radiometer works best. Performance deteriorates in deep water, due to lack of light, and also in very shallow water. The reason for increased CR error in shallow water is probably failure, due to the nearby shadow of the barge, of an underlying assumption of plane-wave illumination.

**ICAM error analysis.** This method does not require standardization with a spectrophotometer or the need of "clean" water to return the total absorption coefficient of the sample. Equation (14) does not include a small term for the absorption which occurs directly in front of the detector. This term can be shown to be about 1% of the $a(532)$ value calculated from (14). Owing to the geometry of the cavity used at Lake Pend Oreille, this term could not be accurately determined and was therefore not included [*Kennedy*, 1992]. The values reported should be viewed as probably low, by about 1%, due to this error. An additional error arises from the assumption that absorption in an air-filled cavity is zero. The assumption of an isotropic field within the cavity sets the upper limit on the absorption coefficient which can be determined. A simple linear analysis, based on the product of the absorption coefficient and the path through the sample, shows that when this product is greater than 0.05, the field at that point will be decreased by about 2%. When the product is 0.01, the field is decreased by less than 0.01% [*Kennedy*, 1992]. The distance from the center of the sample to the outer edge is nominally 0.05 m. If an anisotropy of less than 2% is acceptable, then absorption coefficients of 1.0 $m^{-1}$ or less can be achieved. An improved geometry for the cavity and sample could reduce all of the errors discussed here. Additional error sources, albeit in an earlier configuration of this instrument, are described by *Cleveland and Weidemann* [1993].

**Spectrophotometer error analysis.** Errors in total absorption coefficients estimated from spectrophotometric measurements arise from several sources. The first is the unknown error in values of water spectral absorption obtained from *Smith and Baker* [1981]. Additional errors are associated with separate spectrophotometric determinations of absorption, due to suspended particles and that due to dissolved organic material (gelbstoff).

Calculation of particulate absorption from optical density relies on an empirical algorithm for path length amplification; relative uncertainty associated with this source is approximately 2% for the particular algorithm and spectrophotometer used here [*Cleveland and Weidemann*, 1993]. Potential uncertainty resulting from variability in filtration and inhomogeneous distributions of particles on the filters can be assessed by filtering and measuring replicate samples from each water bottle, but time did not permit adequate sample replication to determine such an estimate during the Lake Pend Oreille optical closure experiment. From other oceanic experiments where replicate filter samples were measured (J. S. Cleveland, unpublished data, 1994), replicability of particulate field samples is approximately 6%. Together, these two sources contribute approximately 6.5% uncertainty (in a mean square sense) to spectrophotometric particle absorption coefficients.

Unfortunately, it is not possible to concentrate gelbstoff, which contributes a low net absorptance at visible wavelengths over the path defined by a 10-cm cuvette. Therefore the resolution limits of the particular instrument used become an important source of uncertainty in spectrophotometric estimates of gelbstoff absorption. The resolution of the Kontron Uvikon 860 spectrophotometer is approximately 0.001 optical density units. For the 10-cm cuvette used here this instrument resolution yields a resolution of 0.02 $m^{-1}$ in absorption units. The overall mean gelbstoff absorption coefficient at 456 nm is 0.132 $m^{-1}$ for this data set. Therefore the 0.02 $m^{-1}$ resolution limit represents 15% of the mean gelbstoff absorption. Sample replicability in gelbstoff absorption, measured during a different experiment (J. S. Cleveland, unpublished data, 1994), was approximately 5%. Combining these two error sources would give a mean square relative uncertainty of approximately 16% in the spectrophotometric gelbstoff absorption coefficients at 456 nm presented here; relative measurement errors in the gelbstoff component of absorption would be progressively larger at 488 and 532 nm, due to the exponential decrease in gelbstoff absorption with wavelength.

## Results

### Meteorological and Limnological Setting

Unusually warm conditions prevailed during the spring of 1992 so that by April 21, when we began our measurements, the lake surface temperature was slightly greater than 6°C, and thermal stratification extended to approximately 50 m. Strong winds on April 29 and 30, 1992, produced strong easterly currents (as indicated by surface drift and instrument wire angles) and upwelling in the vicinity of the barge and throughout Scenic Bay (Figure 1). In this paper we

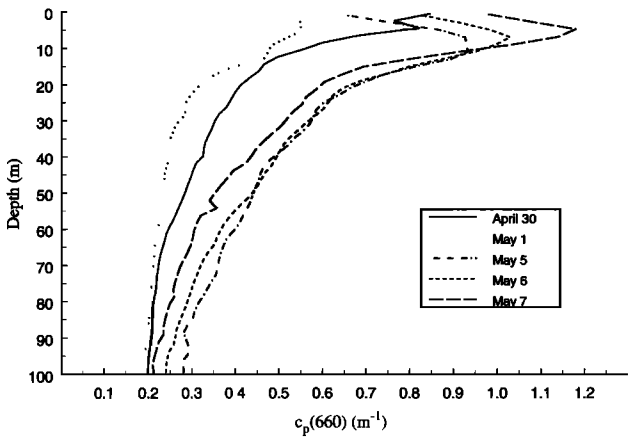


**Figure 4a.** The daily averaged $c_p(660)$ values for the time period covered in this paper.

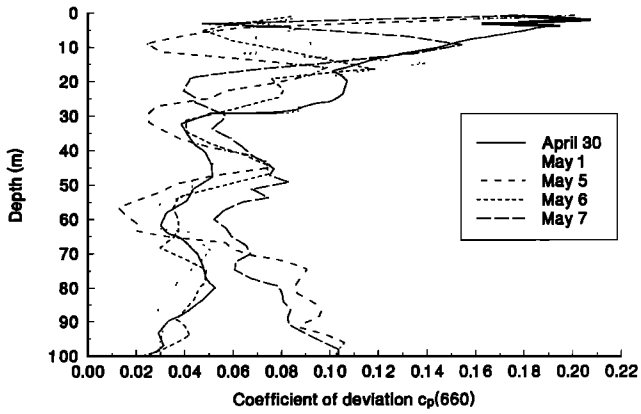


**Figure 4b.** The coefficient of deviation (standard deviation divided by the mean) of the $c_p(660)$ measurements shown in Figure 4a.

present optical measurements over the period of April 30 through May 7. The period of strong wind forcing ended April 30, and associated upwelling reduced the near-surface thermal stratification by the morning of May 1. The surface temperature was reduced from 7.5°C on April 30 to 5.5°C on May 1, and the base of the overall thermocline was depressed to depths between 80 and 100 m. The near-surface mixed layer began to reform on May 1, and the warming trend continued unabated until May 7 when the surface temperature was 10.5°C. Throughout this period a diurnal thermocline was usually present between 10 and 30 m throughout much of the day. The base of the upper portion of the thermocline defining the daily mixed layer was found at the 5°C isotherm, which deepened from approximately 10 m on May 1 to 50 m by May 7. These characteristics were common to the temperature profiles measured with a CTD in the well and with the temperature probe on the TOPS package.

Fluorometers and 660-nm transmissometers were attached to both the CTD and TOPS platforms. The daily averaged profiles of $c_p(660)$ from the two platforms are significantly different only in the upper 5 m of the lake. Comparisons among measurements carried out within the well of the barge and measurements made outside of the barge should then be possible, with the exception of the very near surface waters. Since the CTD operated to greater depths than the TOPS profiler and the differences in the ancillary measurements are confined to the near-surface waters, we will present $c_p(660)$ and fluorometer voltage results only from the instruments mounted on the CTD.

The day-to-day changes in the mean $c_p(660)$ profiles are illustrated in Figure 4a, and the within-day variability is shown in Figure 4b. The transmissometer record indicated that there was a significant amount of natural variability on all timescales. The clearest water measured was on May 1. By May 4 a particle maximum had formed in the upper 20 m. This particle maximum became larger and more sharply peaked over the last 3 days of the experiment. Changes in its depth and magnitude appear in the $c_p(660)$ coefficient of deviation (standard deviation divided by the mean) profile as a local maximum between 10 and 15 m (Figure 4b). The increase in the coefficient of deviation on May 5 and 7 at depths greater than 70 m is caused by the standard deviation remaining constant while the mean value decreased to very small values. Otherwise, the $c_p(660)$ coefficient of deviation remained under 8% for waters greater than 30 m in depth, and often, it was less than 5%.

To estimate the magnitude of short-term variability in particle concentration, we examined the brief time series made at depths where Niskin bottles were attached and removed from the wire during the CTD casts; the longest of these time series, obtained at 65 m on April 30, is illustrated in Figure 5. The maximum amplitude of variability in this 7.5-min time series is one third of the overall variability measured at 65 m throughout the day on April 30; the coefficient of variation for this short time series is approximately 1.5%, compared to a 4% (approximately) daily coefficient of variation (Figure 4b).

Profiles of the daily averaged fluorescence voltage (Figure 6a) show similar shapes and trends as those seen in the $c_p(660)$ profiles (Figure 4a). The coefficients of deviation of the fluorometer voltage profiles (Figure 6b) are larger than those associated with the $c_p(660)$ profiles (Figure 4b).

Vertical profiles of $c_p(660)$, in situ fluorometer voltage, and chlorophyll *a* concentration, obtained from analysis of discrete samples, are used as indicators of the natural variability in particle-related bio-optical properties. Analysis of long-term trends in the above parameters indicate that an

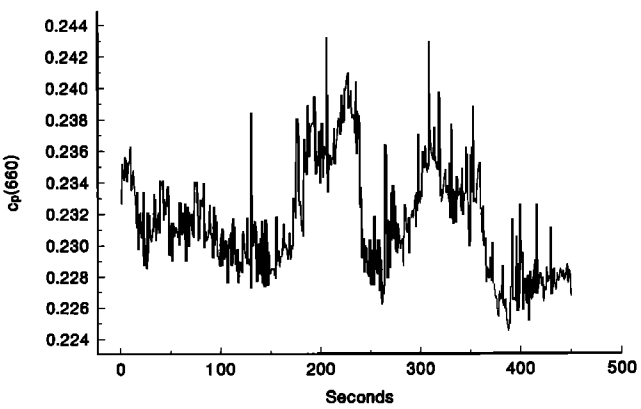


**Figure 5.** A 7.5-min time series of $c_p(660)$ for indication of short-timescale particulate concentration variability.

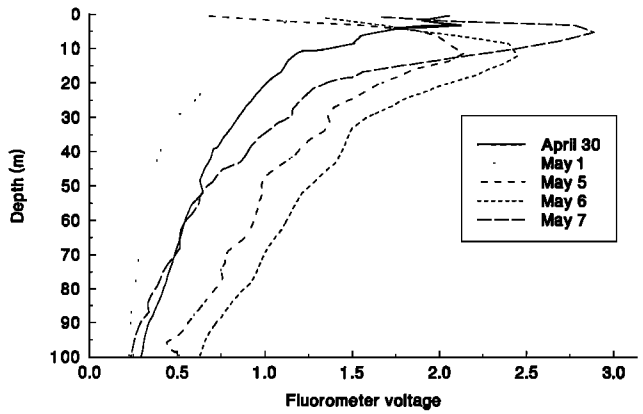


**Figure 6a.** The daily averaged fluorometer voltage for the days covered.

obvious subdiurnal trend in particle properties occurred on only 1 day of the experiment, April 30, when strong winds drove surface waters offshore and produced upwelling throughout much of Scenic Bay. On other days, variability was more random in nature. In the surface waters on April 30, the chlorophyll *a* concentration was 7.58 mg/m$^3$ at 1100 PDT (2 m depth), 5.20 mg/m$^3$ (5 m) at 1600 PDT, and 3.25 mg/m$^3$ (5 m) at 1900 PDT. This trend of decreasing particle concentration is also seen in the transmissometer and fluorometer records, where there was evidence of a decrease down to depths of 30 m.

### Vertical Profiles of Absorption

Vertical profiles of absorption determined by all instruments are illustrated for wavelengths of 456 (Figures 7a–7e), 488 (Figures 8a–8e) and 532 nm (Figures 9a–9e). Figures 7a, 8a, and 9a represent profiles for April 30, with the b–d parts of these figures representing May 1, 5, 6, and 7, respectively. The temporal trends in the optical properties observed on April 30 make the time sequence of the different absorption measurements on that date (Table 2) an important consideration in their interpretation (Figures 7a, 8a, and 9a). On the other dates considered here, bio-optical variability was more random and showed no obvious temporal tendencies throughout the day so that the methods can be compared using the daily mean profiles. Of course, observed spatial

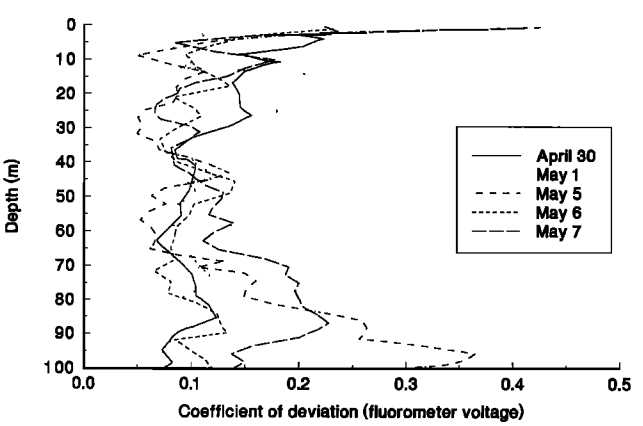


**Figure 6b.** The coefficient of deviation for the daily averaged fluorometer voltage.

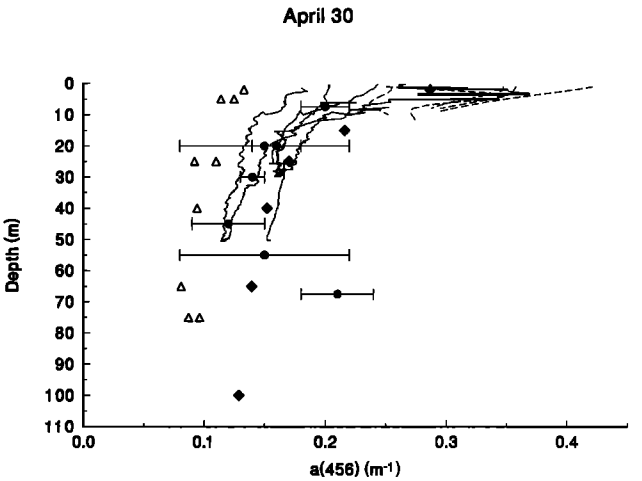


**Figure 7a.** Measurements of $a(456)$ made on April 30 by the reflecting tube absorption meter (RTAM) (solid line), TOPS (dashed line), isotropic point source (IPS) (solid circles, with 1 standard deviation error bars), spectrophotometer (solid diamonds), and integrating cavity absorption meter (ICAM) (open triangles).

and temporal bio-optical variability will contribute significantly to differences in the separately determined means at any given depth. Except for April 30 (Figures 7a, 8a, and 9a), therefore, TOPS and RTAM profiles are shown only as the daily average. Measurements by the IPS (with estimated error bars), spectrophotometer, ICAM, and CR are shown as individual values at discrete depths throughout the day. Refer to Table 1 for a summary of which instrument and wavelength combinations were used on each day.

The only historical data with which we may compare our absorption coefficients from Lake Pend Oreille are those determined using *Tyler*'s [1960] radiance distribution measurements which were made 34 years previous to the present Lake Pend Oreille experiment. The measured radiance distribution were integrated to obtain the vector and scalar irradiance profiles, and vector $K$, needed to compute ab-

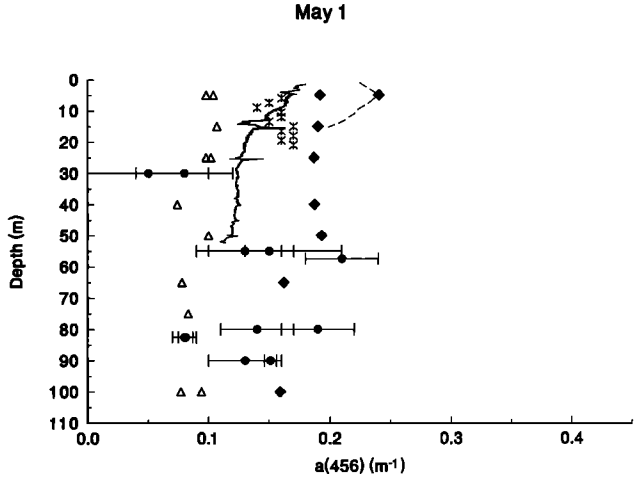


**Figure 7b.** Same as Figure 7a, except the date is May 1. The additional symbols represent the compound radiometer data.

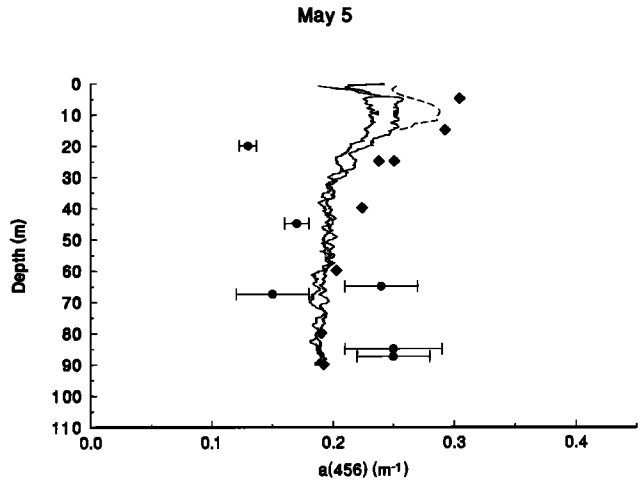


Figure 7c. Same as Figure 7a, except the date is May 5.

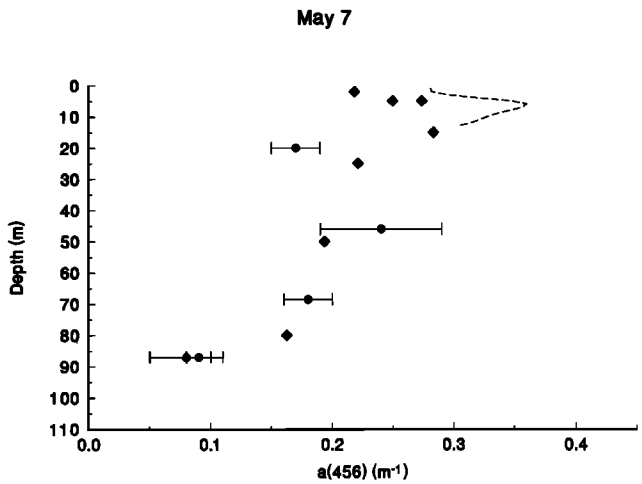


Figure 7e. Same as Figure 7a, except the date is May 7.

sorption from *Gershun*'s [1939, equation (4)]. *Tyler*'s [1960] $a(488)$ values are compared with our own for April 30 in Figure 8a. Tyler's measurements fall within the range of temporal and spatial variabilities observed during the present experiment.

Figure 10 illustrates one example of the comparative profiles of chlorophyll *a* concentration and absorption coefficients for particles and gelbstoff at 456 nm taken from the same set of sampling bottles. The absorption coefficients for particulates and gelbstoff presented were measured using the spectrophotometer. These profiles illustrate that the particulate fractions of absorption and chlorophyll *a* concentration (the primary absorbing material in phytoplankton) follow similarly shaped vertical profiles, which closely mimic those seen in the total absorption profiles measured using most of the methods considered here. Furthermore, the gelbstoff absorption measurements do not follow a profile similar to any of the particle related optical measurements, and there is no evidence in the data to suggest that the dissolved organic concentrations are correlated with suspended particle concentrations. The gelbstoff contribution to the total absorption coefficient increases with depth because of the decrease in particulate absorption.

Data from the ICAM are presented in this paper for April 30 and May 1 (Figures 7a through 9b). ICAM and spectrophotometer samples were obtained from the same Niskin bottles. Absorption values at 456 nm measured with the ICAM were 75% (standard deviation, 12%) lower than those measured with the spectrophotometer. The difference in $a(456)$ between the two laboratory measurements increased with increasing particulate absorption as measured using the spectrophotometer. Agreement between the two laboratory methods improved at 488 nm (48% (standard deviation, 7%)), and differences were essentially unbiased, with much smaller scatter at 532 nm. Similar spectral differences were found in a previous comparison between ICAM and spectrophotometer absorption values [*Cleveland et al.*, 1990].

### Comparison at Specific Depths and Scatterplots

Daily average absorption coefficients for May 1 at 15 and 50 m for the spectrophotometer, ICAM, RTAM, TOPS, IPS, and CR are compared in Table 3. Relative to averages over

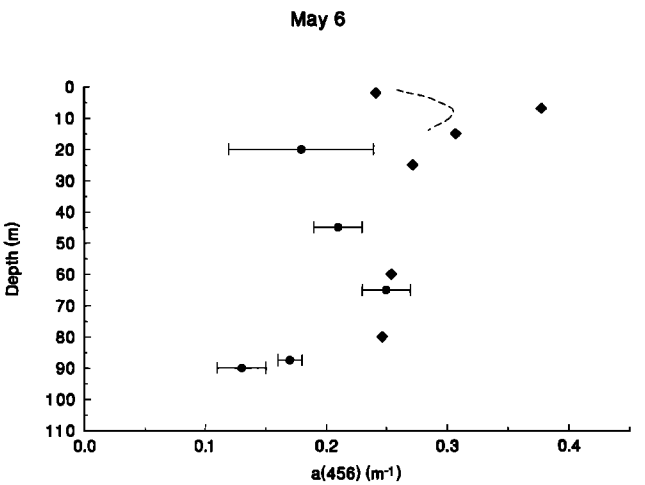


Figure 7d. Same as Figure 7a, except the date is May 6.

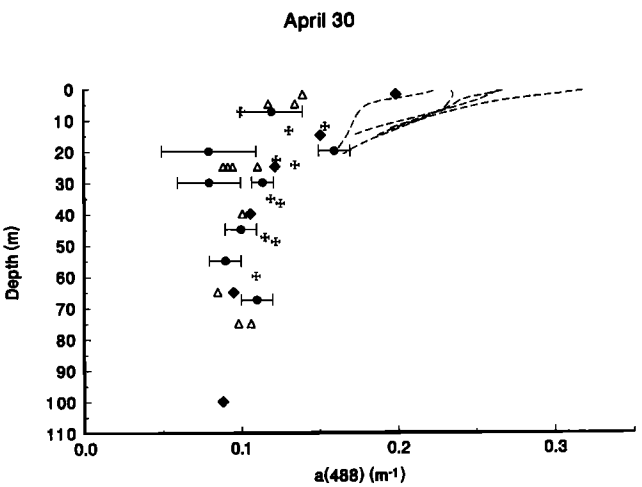


Figure 8a. Same as Figure 7a, except for $a(488)$. The Maltese cross symbols on 30 April 30 are the data from *Tyler* [1960].

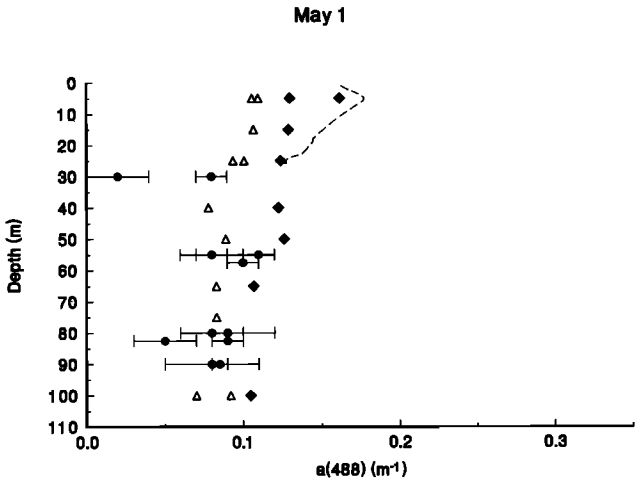


**Figure 8b.** Same as Figure 7b, except for $a(488)$.

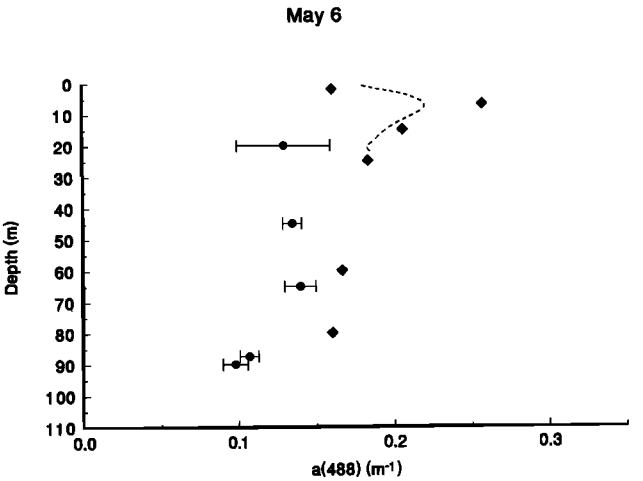


**Figure 8d.** Same as Figure 7d, except for $a(488)$.

all instruments at each depth, at 456 nm the spectrophotometer is 20% to 36% high, ICAM is 46% to 53% low, RTAM is 12% to 17% high, TOPS is 22% high, IPS is 9% high, and CR is 3% high. At 532 nm the spectrophotometer is 1% to 17% low, the ICAM is 1% high, RTAM ranges from <1% low to 6% high, TOPS is 13% high, and IPS is 5% low. This does not imply that the average value is the correct value. It merely highlights potential systematic differences.

Sufficient numbers of paired measurements were made at common depths on May 1–7 to allow direct comparisons of overall deviations in absorption (at all wavelengths) between the TOPS and RTAMs (Figure 11a) and between the spectrophotometer and TOPS (Figure 11b), the RTAMs (Figure 11c), and the IPS and RTAM (Figure 11d). The numbers of absorption pairs measured at common depths on the same days were too few to allow this type of comparison between the other instrument combinations. Mean biases and root-mean-square (RMS) deviations of the TOPS absorption coefficients relative to those of the RTAMs are listed in Table 4 for 456 (May 6 and 7 only) and 532 (May 1, 6, and 7) nm. At these two wavelengths, respectively, TOPS absorption coefficients are biased high by 7% and 4%, and RMS deviations are 6% and 8%, of the associated subsample mean RTAM absorption coefficients; were we to include the May 1, 456 nm subsample, in which the two instruments are obviously biased apart by a fixed 0.05 $m^{-1}$ (Figure 11a), the combined 456-nm mean bias and RMS would increase to 16% and 21%, respectively, of the RTAM mean. Mean biases and RMS deviations, relative to the spectrophotometer spectral absorption coefficients, for the IPS, TOPS, and RTAMs are listed in Table 5. Relative to the spectrophotometer subsample means, at 456 nm, IPS is biased 12% low (25% RMS deviation), TOPS is unbiased (19% RMS deviation), and RTAM is biased 17% low (20% RMS deviation). At 488 nm, IPS is biased 18% low (25% RMS deviation) and TOPS is biased 8% high (19% RMS deviation). At 532 nm, IPS is unbiased (22% RMS deviation), TOPS is 26% high (32% RMS deviation), and RTAM is 19% high (22% RMS deviation). The bias and RMS comparisons in Table 5 are all referenced to the spectrophotometer estimates, simply because it is the only instrument which has enough paired observations (same days and depths) with all three of the others to form a common basis for intercomparisons; we do not suggest that the spectrophotometer absorption estimates should be regarded as a standard.

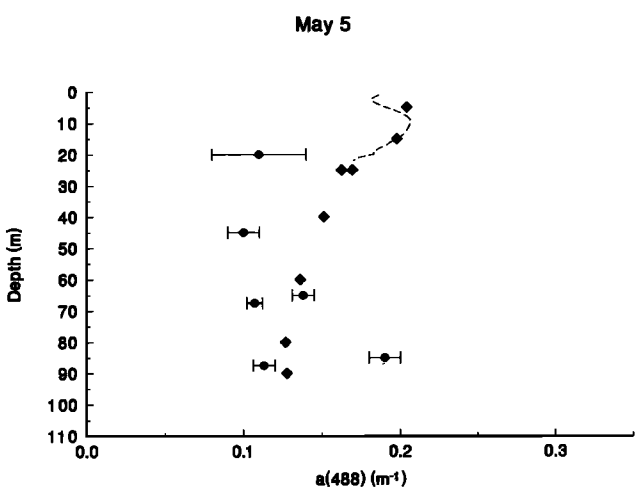


**Figure 8c.** Same as Figure 7c, except for $a(488)$.

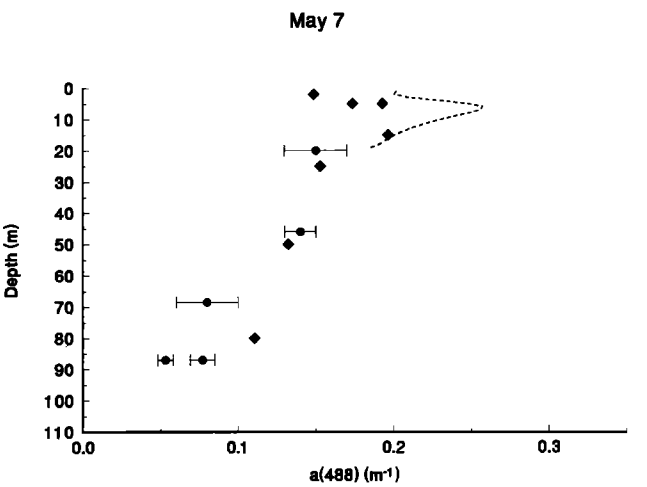


**Figure 8e.** Same as Figure 7e, except for $a(488)$.

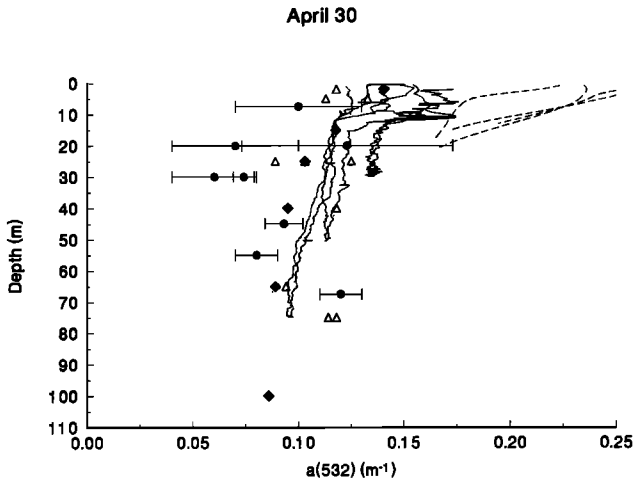


**Figure 9a.** Same as Figure 7a, except for $a(532)$.

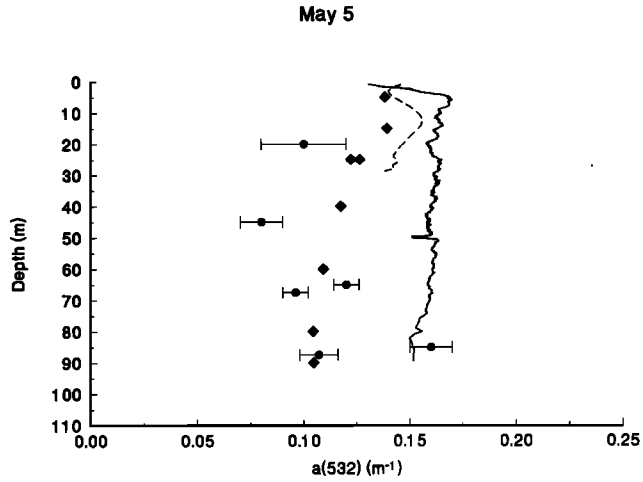


**Figure 9c.** Same as Figure 7c, except for $a(532)$.

## Discussion

### Temporal Variability of Bio-optical Properties

The magnitudes of our absorption values agree remarkably well with those measured by *Tyler* [1960] 34 years earlier (Figure 8a), suggesting that springtime optical properties of Lake Pend Oreille have not changed significantly in the interim. However, Tyler's early April 1958 optical and temperature profiles in March–April 1958 are representative of a vertically well mixed and horizontally homogeneous water column. In contrast to the strong thermal stratification we found in the upper 50 m, Tyler measured a constant temperature of 3.6°C from the surface to 137 m, with a diurnal mixed layer increasing to 4.5°C in the top 1.25 m as late as April 29. Even a casual inspection of the results presented above shows clearly how the vertical structure of optical properties in the lake were strongly affected by the thermally stratified surface layer.

The existence and evolution of the thermally stratified surface mixed layer in Lake Pend Oreille profoundly affected the vertical profile of bio-optical properties during the optical closure experiment. A relatively intense phytoplankton bloom produced strong vertical structure in vertical profiles of particle and pigment concentrations, as documented here by profiles of $c_p(660)$, chlorophyll *a* fluorescence, and extracted chlorophyll *a* concentrations (Figures 4a, 6a, and 10). Profiles of all of these variables show an increase from the surface to a strong maximum in the top 15 m, a decrease with depth below the maximum to approximately surface values between 30 and 50 m, and a continued decrease (approximately exponentially) to constant background values at depths >100 m. The near-surface maxima in daily averages of both $c_p(660)$ and chlorophyll *a* fluorescence initially decreased on May 1, following the April 30 wind event, and then increased monotonically between May 1 and 7 by overall factors of 2.2 and 2.5, respectively (Figures 4a and 6a); the depths of the maxima became progressively shallower each day, from 15 m on May 1 to 5 m on May 7. Chlorophyll *a* concentrations measured in the top 30 m also increased on a daily basis throughout the period. In the water column below 30 m, $c_p(660)$ and fluorescence initially increased after May 1, reached a maximum at all depths between 30 and 100 m on May 5, and then decreased progressively through May 6 and 7 (Figures 4a and 6a). We interpret these sequences as symptomatic of a spring bloom in the top 60 m, which was briefly interrupted by a strong

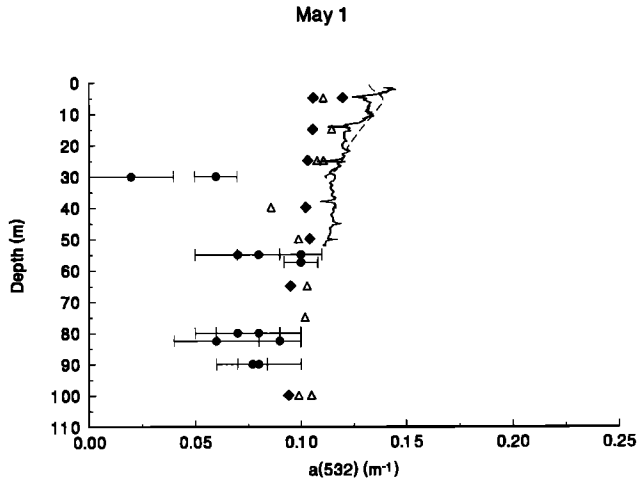


**Figure 9b.** Same as Figure 7b, except for $a(532)$.

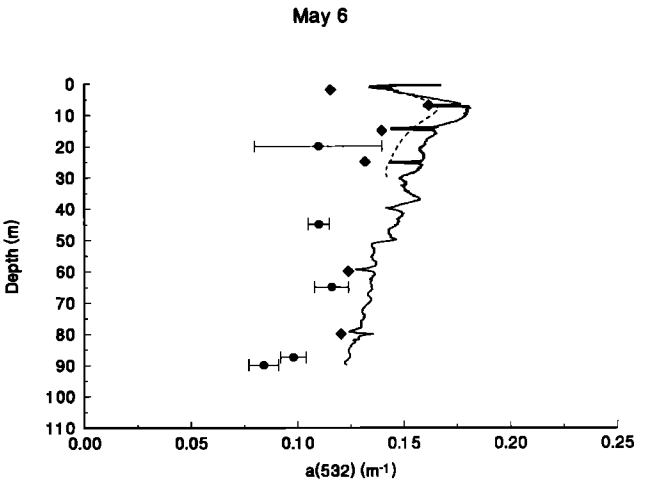


**Figure 9d.** Same as Figure 7d, except for $a(532)$.

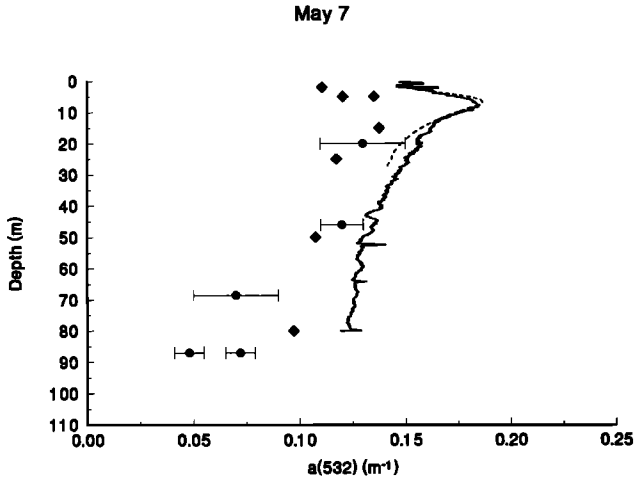


**Figure 9e.** Same as Figure 7e, except for $a(532)$.

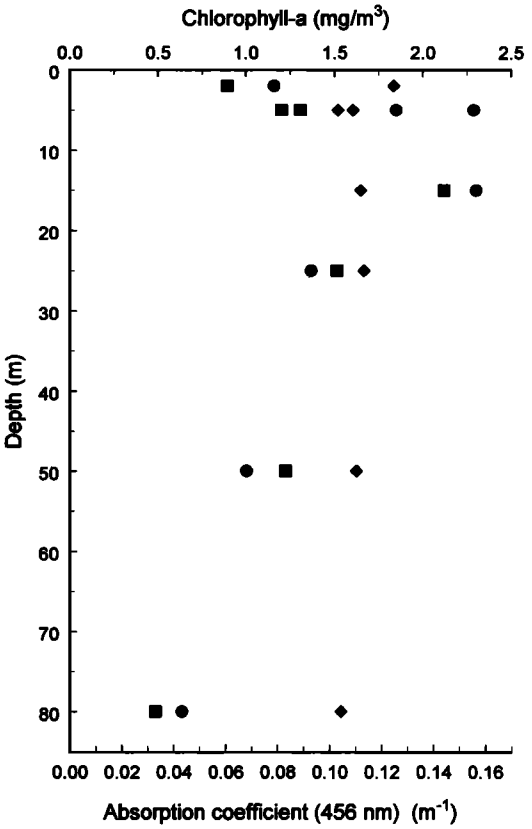


**Figure 10.** The absorption coefficients for the particulate (circles) and gelbstoff (diamonds) components measured using the spectrophotometer and the chlorophyll $a$ concentrations (squares) from the same sample bottles.

wind event which flushed the surface layer out of Scenic Bay and replaced it with deeper water between April 30 and May 1. This was followed by a period of more rapid warming and phytoplankton growth through May 7, which became progressively more confined to the upper 20 to 30 m. Near the end of the period the increased optical density of the surface layer shaded the deeper water column, where reduced productivity levels and sinking combined to produce progressively decreasing particle and chlorophyll $a$ concentrations.

Significant variability of particulate properties is also evident on timescales ranging from diurnal down to a few minutes. Within a given day, $c_p(660)$ and chlorophyll $a$ fluorescence in the water column vary from ±10% to ±>20% in the shallow maxima and in the range of ±4% to ±10% in the water column below 30 m (Figures 4b and 6b). We interpret this diurnal variability as symptomatic of phytoplankton growth and particle sinking associated with the bloom cycle described above, coupled with advective displacements of spatially varying bio-optical profiles in the vicinity of the instrument locations. Short-term variability estimated from time series measurements of $c_p(660)$ at 65 m on April 30 (Figure 5) is approximately 1.5%, which is approximately one third of the corresponding diurnal variability (Figure 4b). Inspection of the CTD cast from which the data for Figure 5 were extracted shows that the base of the seasonal thermocline was at 65 m and that the vertical gradient of $c_p(660)$ at that depth is such that a 3-m random displacement (e.g., due to internal waves) is sufficient to explain the amplitude of the variability in Figure 5. Assuming that a similar mechanism is primarily responsible for short-term variability in the top 30 m, where vertical gradients of bio-optical properties are much larger (Figures 4a and 5a), we may assume that the magnitude of short-term relative variability increases approximately in proportion to diurnal variability (i.e., 3% to 7% in the near-surface maxima).

**Table 2.** Sequence of Absorption Measurements Taken on April 30, 1992

| Time, PDT | Measurement |
|---|---|
| 1100 | water samples at 2, 15, 25, 40, 65, and 100 m for the spectrophotometer, ICAM used water from 2, 40, and 65 m, TOPS casts made |
| 1130 | TOPS cast |
| 1200 | IPS at 15–25, 25–35, 40–50, and 60–75 m |
| 1220 | water sample at 25 m for ICAM |
| 1550 | RTAM to 30 m |
| 1610 | water samples at 5, 25, 75 m for ICAM |
| 1650 | RTAM to 75 m |
| 1900 | IPS at 5–10, 15–25, 25–35, and 50–60 m, water samples at 5, 25, and 75 m for ICAM |
| 2130 | RTAM to 50 m |

Abbreviations are ICAM, integrating cavity absorption meter; TOPS, tethered optical profiler system; IPS, isotropic point source; and RTAM, reflecting tube absorption meter.

The time lapse between the ancillary measurements and individual absorption measurements with different methods was often as large as hours (Table 2), and the measurements were separated horizontally by tens to hundreds of meters. Diurnal and short-term variability clearly contributes significantly to deviations between "daily average" absorption coefficients measured by any pair of instruments. This is especially true in cases where one (or both) of the "averages" being differenced is actually a single observation separated by several hours from the paired "average" measurements; on May 1, for example, the spectrophotometer absorption coefficients were measured from samples taken at 1138 PDT, the CR measurements were made between 1045 and 1340 PDT, the TOPS profiles were measured between 1700 and 1900 PDT, RTAM casts were distributed from 1445

**Table 3.** The Averaged Absorption Coefficients Measured at 15 and 50 m on May 1

| | Spectro-photometer | ICAM | RTAM | TOPS | IPS | CR |
|---|---|---|---|---|---|---|
| | | | *a(456)* | | | |
| 15 m | 0.190 | 0.107 | 0.140 | 0.200 | ··· | 0.170 |
| 50 m | 0.193 | 0.100 | 0.118 | ··· | 0.160 | |
| | | | *a(488)* | | | |
| 15 m | 0.129 | 0.107 | ··· | 0.152 | ··· | ··· |
| 50 m | 0.126 | 0.089 | ··· | ··· | 0.088 | ··· |
| | | | *a(532)* | | | |
| 15 m | 0.108 | 0.115 | 0.123 | 0.129 | ··· | ··· |
| 50 m | 0.104 | 0.099 | 0.113 | ··· | 0.093 | ··· |

Abbreviations are same as Table 2, with CR for compound radiometer. The IPS measurements start at 50 m and extend to 60 m.

to 2100 PDT, and IPS casts were made at 1100 and 1350 PDT.

Profiles of absorption measured in situ with the TOPS and RTAMs are both characterized by vertical structure and spatio-temporal variabilities on weekly, daily, and diurnal timescales (Figures 7–9) similar to those occurring in the $c_p(660)$ and chlorophyll *a* fluorescence profiles. Absorption measurements at fixed depths by the other in situ and laboratory instruments are also consistent with these characteristics of particulate bio-optical profiles (Figures 7–10) but do not resolve the shapes of the vertical profile, nor are the full magnitudes of the shallow maximum usually determined.

### Vertical Profiles

**Spectrophotometer and ICAM.** On most occasions the vertical profiles of the absorption coefficient provided by the spectrophotometer are similar in shape to the $c_p(660)$ and fluorescence profiles with the differences being caused by gelbstoff absorption. The spectrophotometer estimates of the total absorption coefficient did not reproduce the day-to-day variability seen in the fluorescence or $c_p(660)$ profiles. This is, in part, due to the vertical resolution not being fine enough to see the changes in the shape of the particle maximum near the surface and, in part, due to the measured gelbstoff absorption changing independently of the particulate absorption. Since the GF/F filters pass all particles smaller than 0.7 $\mu$m, the gelbstoff absorption estimates obtained with the spectrophotometer from the filtrate probably include some particulate absorption and scattering.

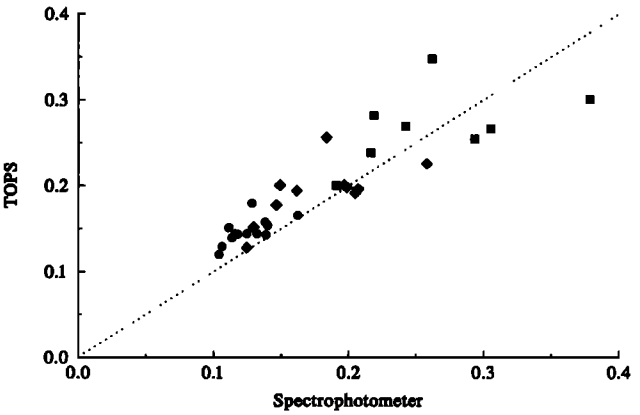


**Figure 11b.** Scatterplot of TOPS versus spectrophotometer data for the absorption coefficient at 456 nm (squares), 488 nm (diamonds), and 532 nm (circles). The data were taken on May 1, 5, 6, and 7.

The ICAM *a*(456) data do not display a significant reduction, as seen in the $c_p(660)$, fluorometer voltage, and chl *a* concentrations seen over the day in the surface waters on April 30 even though it would be expected that *a*(456) would change with the general reduction of particle concentration observed in the ancillary measurements. Direct comparisons of the ICAM results with spectrophotometer measurements made using water from the same sampling bottle were presented earlier in this paper.

**RTAM.** The RTAM measurements provided continuous profiles of the depth structure of the absorption coefficient at 456 and 532 nm. Except for April 30, the RTAM data are presented as a mean profile for the measurements taken throughout the day. The *a*(456) values determined using the RTAM are within the range provided by the other methods. The large- and small-scale temporal and spatial variations observed agree well with the $c_p(660)$ and fluorometer voltage variations. Only on May 5 does the RTAM show a flatter profile than the other parameters. Cavitation in the particular

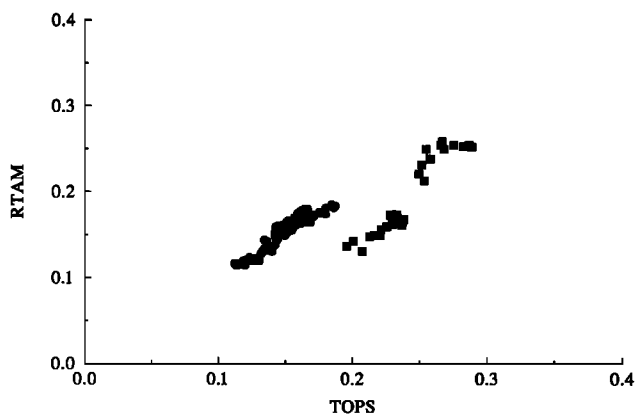


**Figure 11a.** Scatterplot of RTAM versus TOPS data for the absorption coefficient at 456 nm (squares) and 532 nm (circles). The 456-nm data are for May 1, 6, and 7.

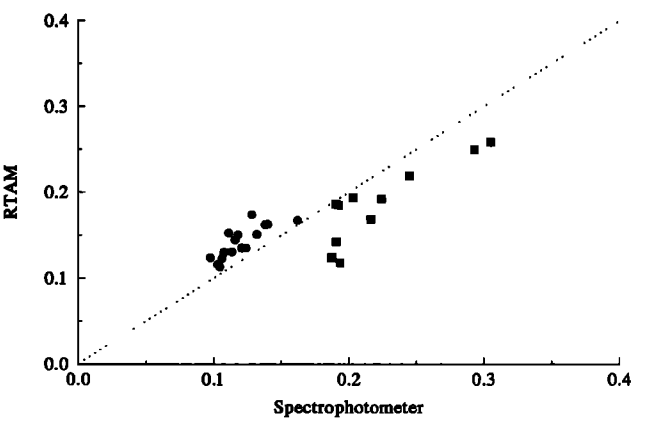


**Figure 11c.** Scatterplot of RTAM versus spectrophotometer data for the absorption coefficient. Symbols for wavelength and observation dates are same as in Figure 11a.

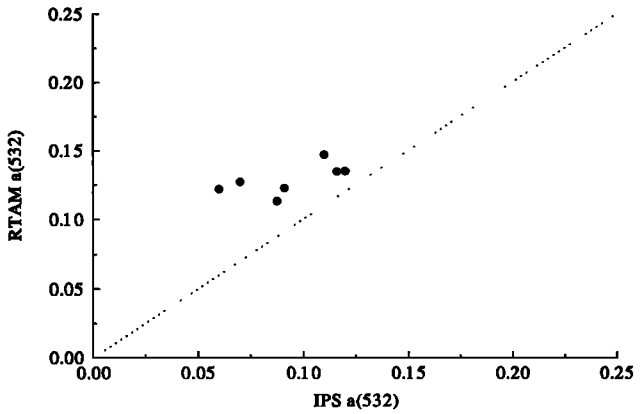


**Figure 11d.** Scatterplot of RTAM versus IPS data for the absorption coefficient at 532 nm. IPS data are from below 30 m. Data were taken on May 1, 6, and 7.

set of instruments used at Lake Pend Oreille may have been the cause of this. The RTAM and spectrophotometer estimates of $a(532)$ differ by 0.015 to 0.025 $m^{-1}$ throughout the experiment. This shows that the structure of the profiles compares very well (to $\pm 0.005$ $m^{-1}$) but that a bias of approximately 0.02 $m^{-1}$ was present. The bias is probably associated with pure water calibrations for the RTAM and purity of reference cell water for the spectrophotometer.

**TOPS.** The absorption coefficients determined using the TOPS data are presented as a mean profile for each day, except on April 30. At all three wavelengths the TOPS measurements are similar in shape to the profiles of $c_p(660)$ and fluorometer voltage. TOPS also reproduced the day-to-day changes in $c_p(660)$ and fluorescence. At 488 nm there is good agreement between the TOPS and the spectrophotometer measurements. The shape and magnitude of the TOPS $a(532)$ profile agree well with the RTAM profiles on most occasions. Except for April 30, the TOPS $a(532)$ measurements are about 10% higher than the spectrophotometer measurements. The $a(532)$ coefficients of deviation are smaller in magnitude than the $c_p(660)$ coefficients of deviation.

**IPS.** At 456 nm on April 30, IPS values compare closely with RTAM, except for an anomolously high value at 70 m which was traced to instrument misalignment. Except for the 70-m data point, the IPS values for this day and wavelength fall between the spectrophotometer and ICAM values. On the other days shown in Figures 7a–7e the IPS system yielded absorption values that varied by as much as a factor of 2, indicating a high degree of instrumental error at this wavelength. This is not surprising, because the lowest signal-to-noise and fewest measurements for the regression fits were at this wavelength. One would therefore expect less variability and better agreement with the other methods at the two longer wavelengths where signals were higher, and this is indeed found to be the case. At 488 nm on April 30 and May 1 there is remarkable agreement among the IPS, spectrophotometer, and ICAM values below about 30 m (Figure 8a). Above 30 m there is still good agreement, but the highly stratified water resulted in an increase in the variability of the measurements. On May 6 and 7 the IPS values tend to be consistently lower than those measured with the spectrophotometer (Figures 8d and 8e).

**CR.** The compound radiometer was only compared with the other absorption measurements during one set of casts. The CR was deployed only on May 1 when clear skies and a calm lake surface made for ideal measurement conditions. In the depth range between 12 and 18 m, where the CR error analysis predicts accurate operation, its absorption coefficients agreed very closely with the mean of the others (Table 3). The CR appeared to measure low absorption values near the surface and high values below 18 m, which is counter to the trends measured by the other in situ instruments (Figure 8a); in absolute magnitude, nevertheless, these values fell well within the range determined by the other instruments for that day.

### Intercomparisons

Comparisons between magnitudes of daily average spectral absorption coefficients measured using the several methods were most complete for the spectrophotometer, RTAMs, IPS, and TOPS. Limited numbers of observations make the comparisons of absorption coefficients measured with the ICAM and CR more anecdotal in nature.

The spectrophotometer measurements provide a convenient common basis for intercomparing the IPS, TOPS, and RTAMS (Figures 11b–11d and Table 5). In general, all of the in situ measurements demonstrate comparable RMS deviations ranging from 17% to 30% relative to the spectrophotometer, with in many cases a mean bias accounting for a large fraction of the deviations. The dominant source of these deviations is the 16% uncertainty in the gelbstoff component of the absorption coefficient determined by the spectrophotometer. All of the other methods measured total absorption, and only the spectrophotometer was used to separate the particulate and dissolved components; unfortunately, its uncertainty in the gelbstoff component is by far the largest instrumental error contribution in this set. The in situ and spectrophotometer particle absorption measurement uncertainties are all $\leq 10\%$, as is the uncertainty associated with environmental variability.

The direct comparisons between TOPS and RTAM absorption coefficients show agreement within 8%, if May 1 $a(456)$ data (which are obviously biased by a fixed offset) are excluded (Figure 11a and Table 4). This agreement is better than the 10% instrumental uncertainty associated separately with each technique.

### The Scale Hypothesis and Other Potential Sources of Error

The "scale hypothesis" of ocean optics asserts that profile measurements of IOP measured over scales of tens of centimeters and representative of volumes ranging from <1

**Table 4.** Mean Biases and RMS Deviations of TOPS Spectral Absorption Coefficients Relative to Those of the RTAMs

| $\lambda$ | $\bar{a}$ | Bias | RMS |
|---|---|---|---|
| 456* | 0.246 | 0.011 | 0.020 |
| 532 | 0.149 | −0.004 | 0.009 |

Variables are $\lambda$, wavelength of light, and $\bar{a}$, mean value of the absorption coefficient.

*Value is for May 1 and 5 only. Mean absorption coefficients are those of RTAM.

**Table 5.** Mean Biases and RMS Deviations of IPS, TOPS, and RTAM Absorption Coefficients Relative to Those of the Spectrophotometer

| | IPS | | | TOPS | | | RTAMs | | |
|---|---|---|---|---|---|---|---|---|---|
| $\lambda$ | $\bar{a}$ | Bias | RMS | $\bar{a}$ | Bias | RMS | $\bar{a}$ | Bias | RMS |
| 456 | 0.203 | −0.019 | 0.052 | 0.263 | −0.007 | 0.052 | 0.219 | −0.039 | 0.045 |
| 488 | 0.135 | −0.024 | 0.034 | 0.178 | 0.015 | 0.033 | ... | ... | ... |
| 532 | 0.109 | −0.009 | 0.022 | 0.126 | 0.021 | 0.037 | 0.119 | 0.021 | 0.024 |

We do not intend to imply that the spectrophotometer is a reference value. It is chosen because it has the most data in common with all the other instruments. Mean absorption coefficients are those of the spectrophotometer.

L to several liters, can be used in radiative transfer models to predict AOPs measured over path length scales of m to tens of meters. In terms of *Gershun*'s [1939, equation (4)], the scale hypothesis states that profiles of absorption measured using small path length (volume) IOP measurements (in this case using the RTAMs, spectrophotometer, and ICAM) are not significantly different from absorption profiles determined using profiles of irradiance measured with instruments having effective path lengths ranging from meters to tens of meters.

Each of the instruments used during the optical closure experiment measures absorption over a different working volume of (or path length in) water. The ICAM and spectrophotometer measure samples representative of 10 L of water collected in a Niskin bottle (assuming that the water in the bottle is well mixed before subsamples are removed) even though each uses smaller subsample volumes. The RTAM measures absorption over a 25-cm path length (volume is approximately 20 mL), but water is pumped continuously through its tube while the instrument traverses approximately 20 cm vertically during each sample. It thus had a vertical resolution of 0.2 $m^{-1}$. The working path lengths of the IPS, TOPS, and CR are determined by the minimum distance over which each can accurately determine the gradient of vector irradiance. The IPS integrates absorption over a 10-m path, in which the water properties are assumed to be homogeneous. Under reasonably stable surface illumination the TOPS system resolves $K$ and $a$ over a few meters and can generally resolve sharp features with vertical scales of approximately 5 m or greater. The CR has a similar working volume to TOPS, but only performs accurately in the narrow depth range between 12 and 18 m.

At the levels of uncertainty in the present absorption comparisons (e.g., <8% for TOPS and RTAM, with similar uncertainties in more anecdotal comparisons between other combinations of instruments) there is no evidence of any systematic deviation between large- and small-volume absorption measurements which would contradict the scale hypothesis. There is also no evidence of systematic differences which might be traced to the 2- to 4-nm differences in center wavelengths and spectral band-pass characteristics between instruments at some nominal wavelengths.

The spectrophotometer and RTAM were both calibrated using pure water filtered by reverse osmosis. The assumed absorption values for the pure water were those of *Smith and Baker* [1981]. Values of the spectral absorption coefficients for pure water have a range of values depending on what source is used [*Tam and Patel*, 1979; *Smith and Baker*, 1981; *Pope*, 1993]. These differences are most pronounced at shorter wavelengths. Systematic biases would be expected were either instrument calibrated using impure reference water or if the assumed absorption values are incorrect. The calibrations of the TOPS and IPS systems are both purely radiometric and therefore are independent of this possible error source. The 8% agreement between TOPS and RTAM (Table 4) is well within the uncertainty of both instrument's error budget and the 10% uncertainty of assumed pure water absorption. Likewise, the 20% to 30% uncertainties in comparisons between the spectrophotometer and both TOPS and IPS absorption (Table 5) are well within the combined instrumental uncertainties, which are dominated by 15% uncertainty (at 456 nm and perhaps 40% uncertainty at 532 nm) in the spectrophotometric gelbstoff absorption estimate. The results do not support a conclusion that impure reference water contributed a significant bias to absorption coefficients measured using either the spectrophotometer or the RTAMs.

Separate measurements of gelbstoff and particulate absorption coefficients were obtained using the spectrophotometer. Since the spectrophotometer measured the particulate component, this component can be compared with the ancillary measurements which provide indications of changes in particle properties. The shape of the particulate absorption profile was similar to the chlorophyll $a$ concentrations (Figure 10), $c_p(660)$, and fluorometer voltage. The profiles of gelbstoff absorption, as may be expected, were not related to any of the ancillary measurements. The gelbstoff absorption becomes increasingly important at greater depths because of the decrease in particulate absorption.

The measurements of $c_p(660)$, fluorescence voltage, and chlorophyll $a$ concentrations do not provide any information about the variability of the gelbstoff concentrations in the water. There is no evidence to indicate that the gelbstoff concentration should be proportional to the particle concentration or that the variability in gelbstoff concentration has the same magnitude or the same time and space scales as the particulate variability. Concentrations of gelbstoff were determined with the spectrophotometer and indicated that gelbstoff absorption was not correlated with particulate absorption. There are only three occasions where measurements of gelbstoff absorption were made twice in a day at the same depth. In these three cases the largest percent change in absorption by gelbstoff was 12.1% for samples taken at 5 m on May 1. The other two cases (May 5, 25 m and May 7, 5 m) showed changes in gelbstoff absorption of 6%. The day-to-day variability in the absorption coefficient attributed to changes in gelbstoff concentration by the spectrophotom-

eter is not always evident in the total absorption coefficients of the other techniques.

## Conclusions

The different techniques for the measurement of the absorption coefficient agreed within ±25% at 532 nm, with decreased agreement at shorter wavelengths, but with far better comparisons between certain methods. When the pure water absorption values are subtracted from all of the measurements at the three wavelengths, the margin of error is roughly constant. The reason is that pure water absorption is a larger fraction of the total absorption at longer wavelengths where better agreement was found. In a purely absorbing medium the methods would likely agree nearly perfectly. Owing to different geometries, the addition of scatterers affects the instruments differently. In the blue part of the spectrum, light sources have smaller outputs and detectors are less sensitive. Therefore comparisons of absorption methodologies (as opposed to specific instrumentation) are best carried out in the green part of the spectrum where purely instrumental problems are smaller. Future comparisons should thus start by making observations at 532 nm. At this wavelength there is sufficient penetration of solar radiation for the techniques that require a natural light field, long path lengths for the isotropic point source, and better signal to noise ratios for the reflecting tube absorption meter. This does not imply that other wavelengths should be ignored. An understanding of the differences in measurement techniques is needed at all wavelengths to compare measurements by investigators using a variety of equipment.

One of the more interesting results is the generally good agreement between the large-volume and small-volume techniques, as well as agreement between in situ measurements and laboratory measurements. There is generally good agreement, on all days and at all three comparable wavelengths, between the IPS method, an in situ large volume measurement, and the spectrophotometer, a bench-top system that uses water samples. On May 1 and 7 there is also good agreement at 532 nm between the RTAM, a small-volume technique, and TOPS, a large-volume technique.

Comparison of the measurements at Lake Pend Oreille is complicated by the natural variability of the lake. The natural variability observed also highlights the difficulty in reporting optical properties of a given water mass. A single or even several profiles are not sufficient to properly define the optical properties of a water mass. For making comparisons of measurements made in a natural environment, the variability of that environment must be taken into account. It is important to be able to track the variability in both particle and gelbstoff properties. Future comparisons of absorption measurements should include some method of providing an intercalibrated reference measurement on all of the absorption measurement platforms, capable of detecting changes in particle and gelbstoff properties. Time series measurements from scales of minutes to days are necessary to properly define the optical properties of a water mass and could also be useful in interpreting the possible effects of natural variability on the different absorption measurements. If the short-timescale variability is large, however, the use of a time series to remove the natural variability from measurements by different techniques will be difficult unless the spatial scale between the location of the measurements is small. We thus recommend that in the future, instruments should be located as much as possible on the same instrument platform.

To improve the comparisons of instruments and the ability to measure the natural variability, new methods will need to be developed that can be used to measure the contributions of the individual components to the total absorption coefficient, both in the laboratory and in situ. As the spectral resolution of the different methods improve, it may be possible to apply inversion techniques to the data in order to identify contributions of the components to the absorption coefficient. It is also possible to filter the input of the RTAM, providing a separation of the components in a manner similar to laboratory techniques. The ability to differentiate the components of the total absorption coefficient will provide methods to check results from the spectrophotometer and help to isolate problem areas of individual measurement techniques. Measurement of component contributions using techniques of all volume scales will improve our understanding of the possible differences that may be associated with use of different sampling volumes.

It should be remembered that it is not possible to make simultaneous measurements on a single volume of water using all of the different methods available because of the differences in sampling volume and time required to obtain a measurement using the different instruments. If all methods are to be compared during a single experiment, then it would be desirable to have waters with little natural variability. Future experiments do not need to include all instrumentation to be in the water at the same time. Comparisons of large-scale techniques, comparison of large- versus small-volume measurements, as well as comparisons between laboratory and in-water techniques, will all improve the understanding of the capabilities of the instrumentation and move us a step closer toward providing comparable measurements of the absorption coefficient by a variety of methods.

Many of the systems used at Lake Pend Oreille were relatively new, and the comparison among systems has shown areas where individual techniques required improvement in design or application (e.g., reduction of cavitation in the reflecting tubes, addition of a reference detector to the IPS, improved geometry for the ICAM). Data analysis techniques were also improved as a result of the experiment. Modifications to the instrumentation and analysis techniques since the Lake Pend Oreille experiment have improved our ability to provide precise, accurate, and dependable measurements of the absorption coefficient with the various techniques.

The Optical Closure Experiment at Lake Pend Oreille provides a benchmark for the measurement of the absorption coefficient of natural waters. Therefore this paper provides a review of most of the available methodologies for the measurement of absorption. Many of the instruments used in this experiment were of relatively new design. This comparison has also highlighted areas where the instrumentation or analysis techniques required improvement. Many of the instruments have been modified in the past 2 years to incorporate changes made obvious by this work. Because of this, we can expect much greater convergence of results at all wavelengths in the near future.

## Notation

$a$ total absorption coefficient, $m^{-1}$.
$a_u$ RTAM measured absorption coefficient, $m^{-1}$.
$a_{part}$ particulate absorption coefficient, $m^{-1}$.
$a_{gelb}$ gelbstoff absorption coefficient, $m^{-1}$.
$a_w$ absorption coefficient of water, $m^{-1}$.
$\hat{a}$ IPS estimated absorption coefficient from a regression fit, $m^{-1}$.
$A_n$ integral moments of the scattering function.
$b$ total scattering coefficient, $m^{-1}$.
$c$ total attenuation coefficient, $m^{-1}$.
$c_p$ particulate attenuation, $m^{-1}$.
$E$ vector irradiance, W $m^{-2}$.
$E_o$ scalar irradiance, W $m^{-2}$.
$E_{u,d}$ upwelling ($u$) and downwelling ($d$) vector irradiance, W $m^{-2}$.
$E_{ou,d}$ upwelling ($u$) and downwelling ($d$) scalar irradiance, W $m^{-2}$.
$E_{ht,l}$ hemispherical irradiance measured on TOPS, top ($t$), lower ($l$), W $m^{-2}$.
$K$ diffuse attenuation coefficient, $m^{-1}$.
$L$ path length, m.
$L_u$ upwelling radiance, W $m^{-2}$ $sr^{-1}$.
OD optical density.
$r$ radial distance, m.
$V$ voltage; volume, $m^3$.
$z$ depth, m.
$\lambda$ wavelength of light, nm.
$\Phi_0$ radiant flux, W.
$\bar{\mu}$ average cosine of the radiance distribution.

**Acknowledgments.** We would like to thank the personnel of the David Taylor Research Center and especially Steve Finley and Steve Payne for the support provided on this project. This work was supported by the Ocean Optics program of the Office of Naval research. W. S. Pegau was also supported by an Augmentation Award for Science and Engineering Research Training.

## References

Bennett, G. T., E. S. Fry, and F. M. Sogandares, Photothermal measurements of the absorption coefficient of water at 590 nm, Ocean Optics 8, *Proc. SPIE Int. Soc. Opt. Eng.*, *637*, 172–180, 1986.

Bricaud, A., A. Morel, and L. Prieur, Absorption by dissolved organic matter of the sea (yellow substance) in the UV and visible domains, *Limnol. Oceanogr.*, *26*, 43–53, 1981.

Cleveland, J. S., and A. D. Weidemann, Quantifying absorption by aquatic particles: A multiple scattering correction for glass-fiber filters, *Limnol. Oceanogr.*, *38*, 1321–1327, 1993.

Cleveland, J. S., R. M. Pope, and E. S. Fry, Spectral absorption coefficients measured with an integrating cavity absorption meter, Ocean Optics 10, *Proc. SPIE Int. Soc. Opt. Eng.*, *1302*, 176–186, 1990.

Doss, W., and W. Wells, Undersea compound radiometer, *Appl. Opt.*, *31*, 4268–4274, 1992.

Elterman, P., Integrating cavity spectroscopy, *Appl. Opt.*, *9*, 2141–2142, 1970.

Fry, E. S., G. W. Kattawar, and R. M. Pope, Integrating cavity absorption meter, *Appl. Opt.*, *31*, 2055–2065, 1992.

Gershun, A., The light field, *J. Math. Phys.*, *18*, 51–151, 1939.

Højerslev, N., A spectral light absorption meter for measurements in the sea, *Limnol. Oceanogr.*, *20*, 1024–1034, 1975.

Jerlov, N. G., *Marine Optics*, Elsevier, New York, 1976.

Kennedy, C. D., Integrating cavity spectral absorption meter, M.S. thesis, Long Mem. Libr., Univ. of New Orleans, New Orleans, La., 1992.

Kiefer, D. A., and J. B. Soohoo, Spectral absorption by marine particles of coastal waters of Baja California, *Limnol. Oceanogr.*, *27*, 492–499, 1982.

Maffione, R. A., R. C. Honey, and R. A. Brown, Experiment for testing the closure property in ocean optics, Underwater Imaging, Photography, and Visibility, *Proc. SPIE Int. Soc. Opt. Eng.*, *1537*, 115–126, 1991.

Maffione, R. A., K. J. Voss, and R. C. Honey, Measurement of the spectral absorption coefficient in the ocean with an isotropic source, *Appl. Opt.*, *32*, 3273–3279, 1993.

Miles, E., and W. H. Wells, Revised results from the underwater compound radiometer, *Off. Nav. Res. Rep. Contract N 00014-88-C-0715*, Dec. 1993. (Available from Tetra Tech Data Syst. Inc., 2451a Impala Dr., Carlsbad, Calif. 92008.)

Moore, C., J. R. V. Zaneveld, and J. C. Kitchen, Preliminary results from an *in situ* spectral absorption meter, Ocean Optics 11, *Proc. SPIE Int. Soc. Opt. Eng.*, *1750*, 330–337, 1992.

Morel, A., Light and marine photosynthesis: A spectral model with geochemical and climatological implications, *Prog. Oceanogr.*, *26*, 263–306, 1991.

Mueller, J. L., Integral method for irradiance profile analysis, *CHORS Tech. Memo. 007-91*, Cent. for Hydro-Opt. and Remote Sens., San Diego, Calif., 1991.

Mueller, J. L., and R. W. Austin, Ocean optics protocols for SeaWiFS validation, *NASA Tech Memo.*, *TM-104566* (5), 43 pp., 1992.

Pope, R. M., Optical absorption of pure water and sea water using the integrating cavity absorption meter, Ph.D. thesis, Texas A&M Univ., College Station, 1993.

Roesler, C. S., M. J. Perry, and K. L. Carder, Modeling in situ phytoplankton absorption from total absorption spectra in productive inland marine waters, *Limnol. Oceanogr.*, *34*, 1510–1523, 1989.

Sathyendranath, S., L. Lazzara, and L. Prieur, Variations in the spectral values of specific absorption of phytoplankton, *Limnol. Oceanogr.*, *32*, 403–415, 1987.

Smith, R. C., and K. S. Baker, Optical properties of the clearest natural waters (200–800 nm), *Appl. Opt.*, *20*, 177–184, 1981.

Sorenson, G., and R. C. Honey, Instrumentation for measuring visibility-limiting characteristics of sea water, Underwater Photo-Optical Instrumentation Applications II, *Proc. Soc. Photo Opt. Instrum. Eng.*, *12*, 115–122, 1968.

Spitzer, D., and M. R. Wernand, *In situ* measurements of absorption spectra in the sea, *Deep Sea Res., Part A*, *28A*, 165–174, 1981.

Strickland, J. D. H., and T. R. Parsons, A practical handbook of seawater analysis, *Bull. Fish. Res. Board Can.*, *167*, 310 pp., 1972.

Tam, A. C., and C. K. N. Patel, Optical absorptions of light and heavy water by laser optoacoustic spectroscopy, *Appl. Opt.*, *18*, 3348–3358, 1979.

Trees, C. C., and K. J. Voss, Optoacoustic spectroscopy and its application to molecular and particle absorption, Ocean Optics 10, *Proc. SPIE Int. Soc. Opt. Eng.*, *1302*, 149–156, 1990.

Tyler, J. E., Radiance distribution as a function of depth in an underwater environment, *Bull. Scripps Inst. Oceanogr.*, *7*, 363–412, 1960.

Voss, K. J., Use of the radiance distribution to measure the optical absorption coefficient in the ocean, *Limnol. Oceanogr.*, *34*, 1614–1622, 1989.

Voss, K. J., and A. L. Chapin, Next generation in-water radiance distribution camera system, Ocean Optics 11, *Proc. SPIE Int. Soc. Opt. Eng.*, *1750*, 384–387, 1992.

Wells, W. H., Techniques for measuring radiance in sea and air, *Appl. Opt.*, *22*, 2313–2321, 1983.

Yentsch, C. S., Measurement of visible light absorption by particulate matter in the ocean, *Limnol. Oceanogr.*, *7*, 207–217, 1962.

Zaneveld, J. R. V., and H. Pak, Some aspects of the axially symmetric submarine daylight field, *J. Geophys. Res.*, *77*, 2677–2680, 1972.

Zaneveld, J. R. V., R. Bartz, and J. C. Kitchen, Reflective-tube absorption meter, Ocean Optics 10, *Proc. SPIE Int. Soc. Opt. Eng.*, *1302*, 124–136, 1990.

Zaneveld, J. R. V., J. C. Kitchen, A. Bricaud, and C. Moore, Analysis of *in situ* spectral absorption meter data, Ocean Optics 11, *Proc. SPIE Int. Soc. Opt. Eng.*, *1750*, 187–200, 1992.

Zaneveld, J. R. V., J. C. Kitchen, and C. C. Moore, Scattering error

correction of reflecting-tube absorption meters, Ocean Optics 12, *Proc. SPIE Int. Soc. Opt. Eng., 2258*, 44–55, 1994.

J. S. Cleveland, J. L. Mueller, and C. C. Trees, Center for Hydro-Optics and Remote Sensing, San Diego State University, 6505 Alvarado Road, Suite 206, San Diego, CA 92120.

W. Doss, R. Stone, and W. H. Wells, Tetra Tech Data Systems, Inc., 2451A Impala Drive, Carlsbad, CA 92008.

C. D. Kennedy and A. D. Weidemann, Naval Research Laboratory, Stennis Space Center, MS 39529.

R. A. Maffione, SRI International, 333 Ravenswood Avenue, Menlo Park, CA 94025.

W. S. Pegau and J. R. V. Zaneveld, College of Atmospheric and Oceanic Sciences, Oregon State University, Ocean Administration Building 104, Corvallis, OR 97331. (e-mail: spegau@oce.orst.edu)

(Received April 25, 1994; revised October 13, 1994; accepted December 22, 1994.)